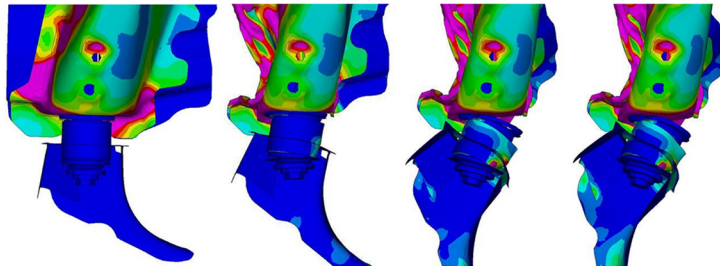




**LUND**  
UNIVERSITY



# **FINITE ELEMENT MODELING OF RUBBER BUSHING FOR CRASH SIMULATION Experimental Tests and Validation**

OSCAR J. CENTENO G.

---

Structural  
Mechanics

*Master's Dissertation*

---



*Department of Construction Sciences*  
Structural Mechanics

ISRN LUTVDG/TVSM--09/5163--SE (1-66)  
ISSN 0281-6679

FINITE ELEMENT MODELING OF  
RUBBER BUSHING  
FOR CRASH SIMULATION  
Experimental Tests and Validation

Master's Dissertation by  
OSCAR J. CENTENO G.

Supervisors:

PhD Per-Erik Austrell,  
Div. of Structural Mechanics

Lic.Eng. Linus Wågström,  
Volvo Car Corporation

Examiner:

Professor Ola Dahlblom  
Div. of Structural Mechanics

Copyright © 2009 by Structural Mechanics, LTH, Sweden.  
Printed by Wallin & Dalholm Digital AB, Lund, Sweden, September, 2009.

For information, address:  
Division of Structural Mechanics, LTH, Lund University, Box 118, SE-221 00 Lund, Sweden.  
Homepage: <http://www.byggmek.lth.se>



To my family... I love you!

“Can’t Never Could”



# Preface

This Master's thesis project has been carried out at the Safety Centre of Volvo Car Corporation, Department of Frontal Impact and Compatibility, Gothenburg, Sweden; and the Division of Structural Mechanics, Lund Institute of Technology, Lund University, during a period of 20 weeks starting March 2009.

I would like to express my gratitude to my supervisors Linus Wågström and Anders Sandahl for all their support, clear guidance and constant feedback during my time at the Department of Frontal Impact and Compatibility. I would also like to thank Petter Winberg for giving me useful ideas and advice concerning LS-DYNA and for his help on finding information.

I would also like to show my appreciation to my supervisor Ph.D. Per-Erik Austrell at the Division of Structural Mechanics, for his support, feedback, ideas and advice throughout this project.

Most importantly, I wish to express a special debt of gratitude to my family and friends, especially my mother and siblings, for always supporting my decisions and giving me guidance throughout this year as an exchange student. Your love and support motivates and encourages me to give my best effort to achieve my goals.

Thank you all

Gothenburg, August 2009

Oscar J. Centeno G.



# Summary

Until recently, the general level of detail in full car crash models has not allowed a physical modeling of rubber bushings with solid elements. This is partly because of the difficulty in modeling the complex characteristic of rubber, but also due to limited understanding of the mechanical properties of rubber materials.

The main focus of this Master's thesis project is to develop a new and improved finite element modeling of rubber bushings for crash simulation, including the model of the bolt joint, which keep the rubber bushing linked to the body structure of the car. The final FE-model has to be able to mimic the real mechanical behavior of the rubber bushing and work effectively in the full-vehicle crash simulation. To achieve this, the program for non-linear dynamic analysis of structures in three dimensions LS-DYNA was used.

In order to validate the final FE-model of the rubber bushing system testing activities and comparisons between the full-vehicle crash simulation with the new and improved FE-model of rubber bushing and the traditional one that often is used in the simulations were made. The experimental activities were carried out in the tower test of the Safety Centre of Volvo Car Corporation.

In the first part of the thesis, comparisons between the finite element analysis and analytical solution of a simple cylindrical model of rubber exposed to shock loading as well as an estimation of the shear modulus  $G$  using the strain energy function of the Yeoh model and an energy balance has been done. The results from the FE-simulation corresponded quite well with the ones from the analytical solution when the Yeoh model is used as the hyperelastic rubber material to model the properties of the rubber.

Regarding the FE-model of the rubber bushing system, the rubber part of the bushing was modeled in a rough way. This is because holes, fillets and other design features within the geometry of the rubber bushing rapidly increase the number of elements needed and, as a result, the computational cost of the analysis and the stability of the model are affected. Therefore, the smaller parts of rubber at the surface of the plastic outer sleeve, aluminum inner sleeve and at the corners while meshing the rubber bushing were not taken into account. The rubber bushing and the screw joint were modeled using 8-node solid elements, 4-node and 3-node shell elements and, 2-node beam elements. The 8-node solid elements were used for the rubber, the aluminum inner sleeve and the bolt head, the 4-node and 3-node shell elements were used for the plastic outer sleeve, the washer, the big nut and the cylindrical casing of the bolt, and the 2-node beam elements were used for the thread and the grip of the bolt. The Yeoh model was used to describe the hyperelastic behaviour of the rubber and for the rest of the model, the evaluated material models were mostly characterized by using elastic piecewise linear plasticity with a specific curve stress/strain and a yield strength. The contacts between metal and metal surfaces and between the rubber and the plastic outer sleeve were solved by using the simple global contact and the LS-DYNA option TIED\_NODES\_TO\_SURFACE\_OFFSET, respectively.

The tightening of the bolt joint was taken into consideration in order to properly describe the friction and contacts between the different parts of the complete rubber bushing system from the beginning of the simulation.

The rubber itself turned out to be just a small part of the complete rubber bushing system, so it was not necessary to use a complex material model to predict the physical response of the rubber. A simple and purely hyperelastic rubber material model where no damping exists was used instead. The Yeoh model worked out to be a stable model at high strain rate and therefore was used with these material parameters:  $C_{10} = 0,55$ ,  $C_{20} = -0,05$ ,  $C_{30} = 0,95$ .

The developed FE-model of rubber bushing system seems to model the nonlinearities in the system as large displacement effects and large deformations, material nonlinearity, and boundary nonlinearities. This is confirmed by the preload in the bolt joint, the contacts, the friction between the different surfaces and the bending and pulling out behaviour of the system working properly at the beginning and during the simulation.

In order to validate the final FE-model of the rubber bushing system it was exposed to different loading cases in the FE-simulations and full-scale tests. The FE-simulations were tested under the same conditions as in the experimental tests in order to have a reference for comparisons. The full-scale impacts and computed deformations agreed qualitatively but they differed in magnitude. The deformations of the rubber bushing system, due to the bending moment, axial force and pulling out between sleeves appear to be similar to what happens in reality. The reason for the inaccuracies may be caused by several approximations in the FE-model and others source of error while carrying out the different experimental test.

An US-NCAP analysis was also performed in LS-DYNA in order to be sure that the final FE-model of the rubber bushing system works properly in the full-vehicle crash simulation. The simulation provided satisfactory results in the full-frontal impact of the car showing a significant improvement in the behavior of the rubber bushing system in comparison with the full-vehicle crash simulation of the traditional FE-model of rubber bushing that is often used in the car.

Finally, the final FE-model of rubber bushing system can be considered reliable and can be used with a high rate of confidence in the full-vehicle crash simulation, since the computational time can be reduced by up to 4 % approximately and when used in the full vehicle crash simulation, this model is more physical and detailed than the traditional one and can better resemble the mechanical behaviour of the real rubber bushing system.

# Contents

<b>Preface</b>	<b>i</b>
<b>1 Introduction</b>	<b>1</b>
1.1 Background	1
1.2 Objective	2
1.3 Methodology	2
1.4 Outline	3
<b>2 Finite element method</b>	<b>5</b>
2.1 Finite element implementation	5
2.1.1 Static analysis	5
2.1.2 Dynamic analysis	6
2.1.3 Stability and time step	7
<b>3 Presentation of rubber and description of constitutive model for rubber</b>	<b>9</b>
3.1 Brief history	9
3.2 General description and characteristic of rubber	10
3.3 Description of constitutive model for rubber	12
3.3.1 The strain energy function	12
3.3.2 Yeoh model. Hyperelastic rubber material model	13
3.3.3 The strain energy functions of compressible materials	14
<b>4 Initial analysis of a simple cylindrical model of drop test</b>	<b>15</b>
4.1 Initial finite element analysis and comparison with analytical solution	15
4.1.1 Finite element model	15
4.1.2 Analytical solution	16
4.2 Estimation of the shear modulus G using the Yeoh model and an energy balance	18
4.3 Results	19
4.4 Analysis of the results	22
<b>5 Development of FE model of the complete test setup of rubber bushing system</b>	<b>23</b>
5.1 Development process of the FE model and software implemented	24
5.2 Geometry and mesh of the model	26
5.3 Material models and assignment of material properties to the model	28

5.4	Contacts in the model . . . . .	28
5.5	Preload . . . . .	29
5.6	Boundary conditions and loads . . . . .	30
<b>6</b>	<b>Laboratory experiments</b>	<b>31</b>
6.1	Equipment and test method . . . . .	31
6.2	Results . . . . .	32
<b>7</b>	<b>FE-simulations: Results and analysis</b>	<b>37</b>
7.1	Results . . . . .	38
7.2	Analysis of the results . . . . .	46
<b>8</b>	<b>Validation</b>	<b>47</b>
8.1	Results . . . . .	48
8.2	Analysis of the results . . . . .	56
<b>9</b>	<b>Conclusions</b>	<b>57</b>

# Chapter 1

## Introduction

*This chapter gives a background to the problem treated in this Master's thesis project, a problem description, methodology description and outline of related work.*

### 1.1 Background

Physics-based simulation is one of the most demanding of all computing tasks. Crash simulation software for explicit finite element analysis is widely used by the automotive industry and must be able to handle large deformations, sophisticated material models, complex contact conditions among multiple components and short-duration impact dynamics. It is more importantly used to enable faster design, reduce expensive testing and as an important tool for assessment and improvement of crashworthiness of cars.

The precision and resolution of the crash simulation models have improved tremendously during the last decade due to extensive method development and the huge increase in computational power. However, several areas are still handled in a simplified way, e.g. with multidimensional spring elements, instead of a more physical modeling. One such area is rubber bushing in engine mounts and wheel suspension.

The suspension components are connected to each other, to the subframe, and to the body structure using rubber bushings. The main function of a complete rubber bushing system is basically to join elements between rigid structures in the system suspension of a car, isolate vibrations through to the chassis and avoid the transmission of noise.

Until recently, the general level of detail in full car crash models has not allowed a physical modeling of rubber bushings with solid elements. This is partly because of the difficulty in modeling the complex characteristic of rubber, but also due to limited understanding of the mechanical properties of rubber materials.

The main focus of this Master's thesis project is to develop a new and improved finite element modeling of rubber bushings for crash simulation, including the model of the bolt joint, which keep the rubber bushing linked to the body structure of the car. To achieve this, the program for non-linear dynamic analysis of structures in three dimensions LS-DYNA was used.

The Master's thesis project has been carried out at the Safety Centre of Volvo Car Corporation, Department of Frontal Impact and Compatibility, situated in Gothenburg, Sweden; and the Division of Structural Mechanics, Lund Institute of Technology. Experimental activities were also carried out in the tower test of the Safety Centre of Volvo Car Corporation in order to verify and validate the final model.

## 1.2 Objective

The rubber bushing system currently used in the crash simulation of the full-vehicle is a simple model with multidimensional spring elements, instead of a more physical model with solid elements. With the physical model, it may be possible to model the nonlinearities in the system as large displacement effects, material nonlinearity, and boundary nonlinearities such as contact and friction.

In nonlinear elasticity, there exist many constitutive models describing the hyperelastic behavior of rubber like materials. These models are available in many modern commercial finite element codes, including LS-DYNA. In the present project it will be proposed a finite element implementation of the Yeoh model, in view of application to contact/impact problems involving large displacement and large deformations.

The main objective of this Master's thesis project is therefore to develop and verify a finite element modeling of rubber bushing for crash simulation. The final FE-model has to be able to mimic the real mechanical behavior of the rubber bushing and work effectively in the full-vehicle crash simulation. In order to validate the final FE-model of the rubber bushing system testing activities and comparisons between the full-vehicle crash simulation with the new and improved FE-model of rubber bushing and the traditional one that often is used in the simulations will be made.

## 1.3 Methodology

This Master's thesis project, carried out in cooperation with the Safety Centre of Volvo Car Corporation and the Division of Structural Mechanics at the Lund Institute of Technology, is divided into several steps:

- Survey literature of the rubber, description of the Yeoh model as a hyperelastic rubber material model and initial finite element analysis of a simple model of rubber.
- Development process of the FE-model of the complete test setup of the rubber bushing system.
- Performance of laboratory experiments and FE-simulations in LS-DYNA/Explicit.
- Post processing and review of the results.
- Validation of the final FE-model of rubber bushing system by comparing the results from the full-scale and simulated test, and verification of the final FE-model in the full-vehicle crash simulation.

## 1.4 Outline

Chapter 2: **Finite Element method** This chapter describes the basic theory of explicit finite element method that has been used for all the structural calculation involved in this project.

Chapter 3: **Presentation of rubber and description of constitutive model for rubber** This chapter briefly describes the history of rubber and its molecular structure, manufacturing process and mechanical properties. The Yeoh model as a hyperelastic rubber material model is also described.

Chapter 4: **Initial analysis of a simple cylindrical model of drop test** This chapter describes and compares the finite element analysis and analytical solution of a simple cylindrical model of rubber exposed to shock loading. An estimation of the shear modulus  $G$  using the strain energy function of the Yeoh model and an energy balance is also done.

Chapter 5: **Development of FE model of the complete test setup of the rubber bushing system** This chapter describes the most important steps that have been taken into account while developing the finite element model of the complete test setup of the rubber bushing system, focusing on the rubber bushing itself.

Chapter 6: **Laboratory experiments** This chapter describes how the different tests of the test setup of the complete rubber bushing system were performed and their corresponding results.

Chapter 7: **FE-simulations: Results and analysis** This chapter describes the results from the corresponding FE-simulations of the experimental tests. Afterward the results and where appropriate, the different shock simulations made are briefly discussed.

Chapter 8: **Validation** A numerical and visual comparison between the FE-simulations and the experimental test made at the test rig of the Safety Centre of Volvo Car Corporation, is made in this chapter. Verification of the final FE-model in the full-vehicle crash simulation is also made in this chapter.



# Chapter 2

## Finite element method

A literature study was carried out to gain a better understanding of the problem, learn more about static and dynamic simulations and get insight into what has been done in different aspect of simulations in the finite element solver LS-DYNA.

Basic theory of explicit finite element method that has been used for all the structural calculations involved in this project will be discussed. More general and specific topics related to the finite element method are given by Belytschko et al. [4] and Cook et al. [5].

### 2.1 Finite element implementation

The information in this section is based mainly on [1] and [3], and only essential equations will be given here.

#### 2.1.1 Static analysis

In most structural problems the inertia effects can be neglected and the problem can be solved assuming that they are quasi-static. The basic equation of equilibrium governing static problems is given by:

$$\mathbf{G} = \mathbf{f}_{int} - \mathbf{f}_{ext} = 0 \quad (2.1)$$

Where  $G$  is known as the residual force vector;  $\mathbf{f}_{int}$  and  $\mathbf{f}_{ext}$  are the internal and external nodal force vectors, respectively, and they are given by the following equations:

$$\mathbf{f}_{int} = \sum_{i=1}^{n_e} \int_{\Omega_e} \mathbf{B}^t \boldsymbol{\sigma} d\Omega_e \quad (2.2)$$

$$\mathbf{f}_{ext} = \sum_{i=1}^{n_e} \int_{\Omega_e} \mathbf{N}^t \rho \mathbf{b} d\Omega_e + \sum_{i=1}^{n_e} \int_{\Gamma_e} \mathbf{N}^t \mathbf{t} d\Gamma_e \quad (2.3)$$

Where  $n_e$  is the total number of finite elements used to model the structure,  $\Omega_e$  is the region occupied by the element,  $\mathbf{B}$  is the strain interpolation matrix,  $\boldsymbol{\sigma}$  is the stress tensor,  $\mathbf{N}$  is the displacement interpolation matrix,  $\rho$  is the density,  $\mathbf{b}$  is the force per unit of mass and  $\Gamma_e$  is the external boundary of each element with a surface traction  $\mathbf{t}$ .

The problem can be both linear and nonlinear. Nonlinearities can arise from large-displacement effects, material nonlinearity and boundary nonlinearities such as contact and friction. If the problem is nonlinear Newton - Raphson method should be used to solve the equation (2.1).

### 2.1.2 Dynamic analysis

In crash simulations, which concern nonlinear dynamic analysis, the quasi-static conditions are obviously not fulfilled due to the fact that a dynamic problem involves loads and responses that vary with time and the duration of loads are small.

When the inertia effects in a problem are important a dynamic analysis must be performed. The equation of equilibrium governing the nonlinear dynamic response of a system of finite elements is:

$$\mathbf{M}\ddot{\mathbf{u}} + \mathbf{f}_{int}(\mathbf{u}, \dot{\mathbf{u}}) - \mathbf{f}_{ext}(t) = 0 \quad (2.4)$$

Where the first term in the equation (2.4) represents the inertial forces generated by the acceleration  $\ddot{\mathbf{u}}$ , the second term represents the internal force expressed as a function of the displacement  $\mathbf{u}$  and the velocity  $\dot{\mathbf{u}}$  ( $\mathbf{f}_{int}(\mathbf{u}, \dot{\mathbf{u}}) = \mathbf{C}\dot{\mathbf{u}} + \mathbf{K}\mathbf{u}$ ). The external force  $\mathbf{f}_{ext}(t)$  is assumed to be a given function of time and is given by the equation (2.3). The mass matrix  $\mathbf{M}$  is given by the following equation:

$$\mathbf{M} = \sum_{i=1}^{n_e} \int_{\Omega_e} \rho \mathbf{N}^t \mathbf{N} d\Omega_e \quad (2.5)$$

In a nonlinear dynamic problem the following set of initial conditions is necessary:

$$\mathbf{u}(0) = \mathbf{u}_0, \dot{\mathbf{u}}(0) = \dot{\mathbf{u}}_0 \quad (2.6)$$

For solving the system of differential equation described in equation (2.4), direct integration is used. LS-DYNA uses a modification of the central difference time integration as an explicit method [1].

The velocities and accelerations using the central difference time integration are obtained from the following equations:

$$\dot{\mathbf{u}}^n = \frac{1}{2\Delta t} (\mathbf{u}^{n+1} - \mathbf{u}^{n-1}) \quad (2.7)$$

$$\ddot{\mathbf{u}}^n = \frac{1}{\Delta t} \left( \dot{\mathbf{u}}^{n+\frac{1}{2}} - \dot{\mathbf{u}}^{n-\frac{1}{2}} \right) = \frac{1}{(\Delta t)^2} (\mathbf{u}^{n+1} - 2\mathbf{u}^n + \mathbf{u}^{n-1}) \quad (2.8)$$

Inserting equation (2.7) and (2.8) from the central difference method in the equation of equilibrium (2.4) the following equation appears:

$$\left( \mathbf{M} + \frac{1}{2} \Delta t \mathbf{C} \right) \mathbf{u}^{n+1} = \Delta t^2 \mathbf{f}_{ext}^n(t) - (\Delta t^2 \mathbf{K} - 2\mathbf{M}) \mathbf{u}^n - \left( \mathbf{M} - \frac{\Delta t}{2} \mathbf{C} \right) \mathbf{u}^{n-1} \quad (2.9)$$

Explicit updating scheme using central difference time integration evaluated the equation(2.9) at the old time step  $t^n$  [1].

From the equations (2.7), (2.8) and (2.9) is possible to note that the accelerations are integrated through time using the central difference rule, which calculates the change in velocity from the middle of the previous increment to determine the velocities at the middle of the current increment. After that, the velocities are integrated through time and added to the displacement at the beginning of the increment to determine the displacement at the end of the increment. Thus, satisfying dynamic equilibrium at the beginning of the increment again provides the accelerations for the new loop.

In order to start the time integration the following equation is used to update the displacement:

$$\mathbf{u}^{-1} = \mathbf{u}^0 - \Delta t \dot{\mathbf{u}}^0 + \frac{\Delta t^2}{2} \ddot{\mathbf{u}}^0 \quad (2.10)$$

Where  $\mathbf{u}^0$  and  $\dot{\mathbf{u}}^0$  are the initial conditions at time  $t = 0$  and from equilibrium is found  $\ddot{\mathbf{u}}^0$  as explained before.

### 2.1.3 Stability and time step size

The explicit method requires small time increment to produce accurate results, depending on that the accelerations in the central difference formula are assumed to be nearly constant. To know that the simulation provide accurate results the time step must be smaller than a critical value  $\Delta t$  known as the stability limit (without damping):

$$\Delta t \leq \frac{2}{w_{max}} \quad (2.11)$$

Where  $w_{max}$  is the maximum natural frequency of the finite element mesh.

The time step can be estimated roughly using the formula [1]:

$$\Delta t = 0.9 \frac{l}{c} \text{ (solid, shell, beam)} \quad (2.12)$$

Where  $l$  is the smallest element dimension and  $c$  is the speed of sound in the material, which equation depends on the type of element. Shell thickness and beam section dimensions are ignored when finding  $l$ . Rigid elements are not included.

The minimum element size for each type of element can be determined in an approximate way using the corresponding equation of time step size. In areas which don't deform very much it is recommended to increase the size of the element to reduce the number of degrees of freedom in the FE model. This will reduce the time needed to perform one simulation of the finite element model.

On the other hand, LS-DYNA adds mass to nodes that has a time step smaller than the user defined level. By adding mass the speed of sound in the material, which is proportional to  $\sqrt{E/\rho}$ , is reduced and then the critical time step given by the equation (2.12) is increased. The process of adding mass induces errors in the solution of the simulation but in most cases

the added masses are very small in comparison and cause a small global error.

# Chapter 3

## Presentation of rubber and description of constitutive model for rubber

The mechanical behaviour of rubber-like materials is usually modeled as hyperelastic constitutive models. Hyperelasticity is usually described with a strain energy function. For this project, the Yeoh model will be used as the strain energy function to solve the problem.

The decision to use the Yeoh model as the hyperelastic rubber material model to solve the problem is based mainly on the work done and supervised by Per-Erik Austrell [9], [12].

The Yeoh model is a multiparameter polynomial function. The ability to adjust the strain energy function to a stress-stretch curve will increase with more parameters and a higher order of the polynomial. The constants of this function can be obtained approximately from the initial shear modulus or more accurately by a simple least squares method from a stress strain curve of a laboratory test. Based on the conclusions of [12], the Yeoh model is very stable in simulations and during the shock phase the model gives more accurate results than a visco-hyperelastic model where damping exist

This chapter therefore first briefly describes the history of rubber and its molecular structure, manufacturing process and mechanical properties, and then describes the Yeoh model as a hyperelastic rubber material model. For more detailed information about rubber material models the reader is referred to [12]-[15].

### 3.1 brief history

The history of rubber is described in the *Columbia Encyclopedia* [10] as follow: Pre-Columbian peoples of South and Central America used rubber for balls, containers, and shoes and for waterproofing fabrics. Although it was mentioned by Spanish and Portuguese writers in the 16th century, rubber did not attract the interest of Europeans until reports about it were made (1736–51) to the French Academy of Sciences by Charles de la Condamine and François Fresneau. Pioneer research in finding rubber solvents and in waterproofing fabrics was done before 1800, but rubber was used only for elastic bands and erasers, and these were made by cutting up pieces imported from Brazil. Joseph Priestley is credited with the discovery c.1770 of its use as an eraser, thus the name rubber.

The first rubber factory in the world was established near Paris in 1803 and the first in England by Thomas Hancock in 1820. Hancock devised the forerunner of the masticator (the rollers through which the rubber is passed to partially break the polymer chains), and in 1835 Edwin Chaffee, an American, patented a mixing mill and a calender (a press for rolling the rubber into sheets).

In 1823, Charles Macintosh found a practical process for waterproofing fabrics, and in 1839 Charles Goodyear discovered vulcanization, which revolutionized the rubber industry. In the latter half of the 19th century the demand for rubber increased with use of rubber insulation by the electrical industry and the invention of the pneumatic tire.

During World War I, Germany made a synthetic rubber, but it was too expensive for peacetime use. In 1927 a less costly variety was invented, and in 1931 neoprene was made, both in the United States. German scientists developed Buna rubber just prior to World War II. When importation of natural rubber from the East Indies was cut off during World War II, the United States began large-scale manufacture of synthetic rubber, concentrating on Buna S. Today synthetic rubber accounts for about 60% of the world's rubber production.

## 3.2 General description and characteristic of rubber

Rubber compounds are generally composed of a base rubber, a filler, e.g. carbon black, and a curing agent. Additional components may include antioxidants, adhesion agents, flame retardant agents and special process-enhancing chemical additives. Common physical properties measured in compounds include hardness, ultimate tensile strength, ultimate elongation, rebound resilience, aging resistance, tear resistance, weather resistance and fatigue resistance.

Every ingredient of a rubber recipe may affect these physical properties both independently and dependently of each other. The mixing and curing process is also critical in determining these properties. Changes to improve one compound property may affect other properties, positively or negatively [11].

The important process of vulcanization converts the plastic raw elastomeric material into a solid and elastic consistency. Vulcanization is a chemical process where the long molecular chains are linked together and thereby form a stable and more solid molecular structure. The cross linking is enabled by a small amount of sulfur that is mixed with the plastic raw material. When the mixture is heated to about 170°C the vulcanization process starts and cross-links are formed, connecting the molecular chains [9].

Fillers such as carbon-black are added in order to increase the stiffness of the material or, for some applications, to increase the resistance to wear. Carbon-black consists of very small particles of carbon (20 nm – 50 μm) that are mixed into the raw rubber base before vulcanization. The filler and the elastomeric material are not chemically joined; they are separate phases in the vulcanized rubber connected only by cross-links. The rubber phase forms a continuous network, and the filler material forms agglomerates inside the rubber network. The material is thus a two-phase material made from constituents with completely different mechanical properties [9].

Vulcanization and shaping are combined in the so-called moulding process. The rubber-filler mix is inserted into the mould cavity and heated to the appropriated temperature, and the vulcanization starts. The curing time is dependent on the temperature, the size of the unit and on how well heat is transferred to the unit. In technical applications are often composed of both rubber and steel. The attached steel parts are used to connect the rubber unit to other structures or to increase the stiffness of the unit. It is possible to attach steel parts to the rubber material in the moulding process. The steel parts are bonded, very efficiently, to the rubber.

The bond is stronger than the rubber material itself in the sense that a rupture in a manufactured rubber-steel unit usually occurs in the rubber and not at the bonding surface between rubber and steel [9].

The capacity to recover from large deformations is one of the distinguishing mechanical properties of rubber. Certain rubber compounds can recover from nominal strains of up to 600%. What is particular about this behaviour is the nonlinear stress-strain relationship encountered throughout such deformation. It is generally characterized by initial softening, then sudden stiffening as the material approaches its elongation limit.

The behaviour of rubber material is very time dependent. The strain rate has a major effect on the stiffness, which increase dramatically in rapid process. This behaviour can partly be described as viscoelastic. The major part of the relaxation occurs in a very short time. The relation between the shear modulus and the bulk modulus is large, the bulk modulus is usually 1000-2000 times higher than the shear modulus. This makes rubber nearly incompressible. Thus in many cases the approximation of incompressibility is quite appropriate [9].

The stiffness of the rubber is also affected by other factors. At a harmonic load, the frequency and the amplitude have a great influence. A higher frequency will increase the stiffness, while increased amplitude will decrease the stiffness [12]. The temperature is an important factor as well. At temperatures over 0°C, the stiffness will be relatively constant, provided it is not close to the vulcanization temperature. At lower temperature, the stiffness will be remarkably higher. Below -60°C to -80°C the rubber will be in a glassy state [9].

When the unloading path of a stress-strain curve is different from the loading path a phenomenon called hysteresis occurs. Unfilled rubber shows little hysteretic behaviour as it usually follows practically the same path during loading and unloading. For filled rubber, the loading stress-strain path is considerably different from the unloading path.

Filled rubber is also known to undergo strain-induced stress-softening, also known as Mullin's effect. The phenomenon is described as decreasing stiffness with strain, sometimes identified as damage. This means that the first time a material is stretched to a certain level the stress will be higher than the next time the material is stretched to the same level. The reason is that the cross-links between the molecular chains break down. However, if the material is allowed to rest there will, however, be some recovery [12].

### 3.3 Description of constitutive model for rubber

The Yeoh model as a hyperelastic material model is discussed in this section.

The information in this section is based mainly in [9], [12]-[15].

#### 3.3.1 The strain energy function

A constitutive material law is said to be hyperelastic if it is defined by a strain energy function. The strain energy density function is defined in a general way according to the following expression:

$$W(E_{ij}) = \int_0^{E_{ij}} S_{ij}(\widetilde{E}_{ij}) d\widetilde{E}_{ij} \quad (3.1)$$

Where  $W$  is the strain energy;  $E_{ij}$  is the Green-Lagrange strain tensor; and  $S_{ij}$  is the second Piola-Kirchoffs stress tensor.

Differentiation of the strain energy  $W$  with respect to the Lagrangian strain gives the energy conjugate second Piola-Kirchoff stress:

$$S_{ij} = \frac{\partial W}{\partial E_{ij}} = 2 \frac{\partial W}{\partial C_{ij}} \quad (3.2)$$

The Cauchy-Green strain tensor  $\mathbf{C}$  and the Green-Lagrange strain tensor  $\mathbf{E}$  are defined as:

$$\mathbf{C} = \mathbf{F}^T \mathbf{F}, \quad \mathbf{E} = (\mathbf{C} - \mathbf{I})/2 \quad (3.3.a)$$

$$\mathbf{F} = \begin{bmatrix} \frac{\partial x}{\partial X} & \frac{\partial x}{\partial Y} & \frac{\partial x}{\partial Z} \\ \frac{\partial y}{\partial X} & \frac{\partial y}{\partial Y} & \frac{\partial y}{\partial Z} \\ \frac{\partial z}{\partial X} & \frac{\partial z}{\partial Y} & \frac{\partial z}{\partial Z} \end{bmatrix} = \begin{bmatrix} \frac{\partial \mathbf{r}}{\partial X} & \frac{\partial \mathbf{r}}{\partial Y} & \frac{\partial \mathbf{r}}{\partial Z} \end{bmatrix} \quad (3.3.b)$$

Where  $\mathbf{F}$  is the deformation gradient tensor,  $\mathbf{I}$  is the identity tensor and  $\mathbf{r}$  is the deformed configuration.

A measure of deformation is given by stretch:

$$\lambda = \frac{ds}{dS} \quad (3.4)$$

Where  $ds$  is the length of the arbitrary position vector ( $\mathbf{r}$ ) and  $dS$  is the length of the reference position vector ( $\mathbf{r}_0$ ).

The principal stretches  $\lambda_i$  can be calculated as the eigenvalue to the right Cauchy Greens deformation tensor  $C_{ij}$ . The principal stretches can be used to calculate the strain invariants  $I_i$

$$I_1 = \text{tr}(\mathbf{B}) = \lambda_1^2 + \lambda_2^2 + \lambda_3^2 \quad (3.5.a)$$

$$I_2 = \frac{1}{2}(\text{tr}(\mathbf{B})^2 - \text{tr}(\mathbf{B}^2)) = \lambda_1^2 \lambda_2^2 + \lambda_1^2 \lambda_3^2 + \lambda_2^2 \lambda_3^2 \quad (3.5.b)$$

$$I_2 = \frac{1}{2}(tr(\mathbf{B})^2 - tr(\mathbf{B}^2)) = \lambda_1^2 \lambda_2^2 + \lambda_1^2 \lambda_3^2 + \lambda_2^2 \lambda_3^2 \quad (3.5.b)$$

$$I_3 = det(\mathbf{B}) = \lambda_1^2 \lambda_2^2 \lambda_3^2 \quad (3.5.c)$$

There are different stress tensors. The stress tensor for a hyperelastic, isotropic and incompressible material, which represents the true stress, is called Cauchy stress tensor  $\sigma_{ij}$  and is given by the following equation:

$$\boldsymbol{\sigma} = 2 \left( \frac{\partial W}{\partial I_1} + I_1 \frac{\partial W}{\partial I_2} \right) \mathbf{B} - 2 \frac{\partial W}{\partial I_2} \mathbf{B}^2 + p \mathbf{I} \quad (3.6)$$

Where  $\mathbf{B} = \mathbf{F}^T \mathbf{F}$  is the left Cauchy-Greens deformation tensor and  $p$  is an independent field quantity.

### 3.3.2 Yeoh model. Hyperelastic rubber material model

The Yeoh model, also known as the third-order reduced polynomial form, describes isotropic incompressible rubber-like materials. The strain energy density function  $W$ , implemented in most of the general finite element programs capable of handling hyperelastic materials is given by the following equation:

$$W(I_1, I_2, I_3) = \sum_{i,j,k=0}^{\infty} C_{ijk} (I_1 - 3)^i (I_2 - 3)^j (I_3 - 1)^k \quad (3.7)$$

If total incompressibility is assumed ( $I_3 = 1$ ) the equation (2.7) changes to:

$$W(I_1, I_2) = \sum_{i,j=0}^{\infty} C_{ij} (I_1 - 3)^i (I_2 - 3)^j \quad (3.8)$$

Where  $C_{ij}$  are unknown constants. The explicit version of this equation, with terms having an index sum less or equal to three, is written as:

$$\begin{aligned} W = & C_{10}(I_1 - 3) + C_{01}(I_2 - 3) + C_{20}(I_1 - 3)^2 + C_{11}(I_1 - 3)(I_2 - 3) + C_{02}(I_2 - 3)^2 \\ & + C_{30}(I_1 - 3)^3 + C_{21}(I_1 - 3)^2(I_2 - 3) + C_{12}(I_2 - 3)^2(I_1 - 3) \\ & + C_{03}(I_2 - 3)^3 + \dots \end{aligned}$$

The third order of deformation material is found by taking terms that include  $I_1$ ,  $I_2$ ,  $I_1^2$ ,  $I_1^3$  and  $I_1 I_2$ :

$$W = C_{10}(I_1 - 3) + C_{01}(I_2 - 3) + C_{20}(I_1 - 3)^2 + C_{11}(I_1 - 3)(I_2 - 3) + C_{30}(I_1 - 3)^3 \quad (3.9)$$

The dependence on the second invariant is very weak for carbon-black filled natural rubbers [9]. Thus, by leaving out terms in (3.8) that include  $I_2$  it is possible to get the strain energy function for the Yeoh model, which gives a good fit to experiment carried out on filled rubbers. Consequently, this strain energy function is given by the following expression:

$$W(I_1) = C_{10}(I_1 - 3) + C_{20}(I_1 - 3)^2 + C_{30}(I_1 - 3)^3 \quad (3.10)$$

The rubber material parameter  $C_{ij}$  can be obtained approximately from the initial shear modulus. The approximate relations are given by the following equations:

$$C_{10} = \frac{G}{2}; C_{20} = -\frac{G}{20}; C_{30} = \frac{G}{200} \quad (3.11)$$

It is important to know that the parameters  $C_{10}$  and  $C_{30}$  influence the behaviour of the rubber at low and high strain rate, respectively.

### 3.3.3 The strain energy function of compressible materials

The explicit finite element code LS-DYNA cannot handle complete incompressibility in rubber-like materials, the material model must for this reason be modified. For numerical purpose, it proves useful to separate the deformation in volumetric and isochoric parts by a multiplicative split of a deformation gradient as:

$$\mathbf{F} = \mathbf{F}^{iso} \mathbf{F}^{vol}, \text{ with } \mathbf{F}^{vol} = J^{1/3} \mathbf{I}, \mathbf{F}^{iso} = J^{-1/3} \mathbf{F} \quad (3.12)$$

This decomposition is such that  $\det(\mathbf{F}^{iso}) = 1$ . It is easy to see that  $\mathbf{F}^{iso}$  and  $\mathbf{F}$  have the same eigenvectors. The relative volume change  $J$  is equal to 1:

$$\lambda_1 \lambda_2 \lambda_3 = 1 \quad (3.13)$$

In order to use the same equation described above the principal stretches are modified in the following way:

$$\lambda_i^* = J^{-1/3} \lambda_i, \quad \lambda_1^* \lambda_2^* \lambda_3^* = 1 \quad (3.14)$$

The invariants will then be defined as:

$$I_1^* = I_1 J^{-2/3} = I_1 I_3^{-1/3} \quad (3.15.a)$$

$$I_2^* = I_2 J^{-4/3} = I_2 I_3^{-2/3} \quad (3.15.b)$$

$$I_3^* = 1 \quad (3.15.c)$$

In order to enforce the incompressibility constraint, another term is added so as to obtain finally the following strain energy function:

$$W(I_1^*, J) = \sum_{i=1}^3 C_{i0} (I_1^* - 3)^i + \sum_{k=1}^3 1/d_k (J - 1)^{2k} \quad (3.16)$$

Where  $C_{i0}$  and  $d_k$  are material constants. By expressing the strain energy density in terms of the invariants of the right Cauchy-Green strain tensor, the equation (3.2) becomes:

$$\mathbf{S} = 2 \left( \sum_{i=1}^3 i C_{i0} (I_1^* - 3)^{i-1} \right) J^{-2/3} \left[ \mathbf{I} - \frac{I_1}{3} \mathbf{C}^{-1} \right] + \left( \sum_{k=1}^3 2k/d_k (J - 1)^{2k-1} \right) J \mathbf{C}^{-1} \quad (3.17)$$

The Cauchy stress (or true stress) tensor  $\boldsymbol{\sigma}$  is calculated from the second Piola-Kirchoff stress tensor  $\mathbf{S}$  [16]:

$$\boldsymbol{\sigma} = \frac{1}{J} \mathbf{F} \mathbf{S} \mathbf{F}^T \quad (3.18)$$

# Chapter 4

## Initial analysis of a simple cylindrical model of drop test

An initial finite element analysis was performed to get a better understanding of the Yeoh material model that was described in chapter 2. An estimation of the shear modulus  $G$  using the Yeoh model and balance energy was also obtained.

The finite element simulation of a simple cylindrical model exposed to shock loading will be described in this chapter, see figure 4.1. An analytical solution is also obtained for the same system and under the same loading conditions. The results from the FE-simulations and the analytical solution are compared. Then, the estimation of the shear modulus  $G$  is done. In the end, all the results are analyzed.

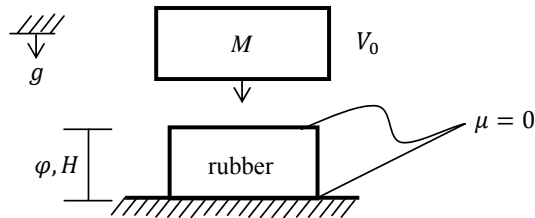


Figure 4.1: Configuration of the simple system of drop test exposed to shock loading. The rubber is a cylinder with  $\varphi = 25$  mm and  $H = 24$  mm.

### 4.1 Initial finite element analysis and comparison with the analytical solution

#### 4.1.1 Finite element model

The simple cylindrical model of the rubber has the configuration shown in figure 4.1, it was modeled in the finite element code LS-DYNA using 8-node solid elements with 48 degrees of freedom. The brick elements are fully integrated. The simple model is confined between two rigid surfaces. The bottom surface corresponds to the base or floor and it is constrained in all directions. The upper surface corresponds to the impactor mass and it is constrained in all directions except for the vertical direction, allowing the impactor mass to fall.

Due to the fact that it was not possible to carry out the experimental test in order to identify the rubber material parameters, the Yeoh model was used with the following rough estimation of the rubber material parameters  $C_{10} = 0,55$  MPa,  $C_{20} = -0,05$  MPa and  $C_{30} = 0,015$  MPa. Such estimation was obtained from the hardness of the rubber: 52 shore A. The mass density and Poisson's ratio were assumed to be  $\rho = 1,1 \cdot 10^{-6}$  Kg/mm<sup>3</sup> and  $\nu = 0,499$ . Lubricated surfaces ( $\mu = 0$ ) have been assumed in the model to guarantee the condition of homogeneous compression and to be able to compare the results with the ones from the analytical expression, which does not consider energy lost by friction.

The system was exposed to different loading conditions. The initial velocity  $V_0$  and the impactor mass  $M$  were varied between 0,5 – 2 m/s and 1 – 5 Kg, respectively. The force as a function of the time in the moment of maximum compression of the cylindrical rubber, see figure 4.4, was used to construct the diagram of maximum force as a function of the time, see figure 4.5, in order to compare the results with the analytical solution.

### 4.1.2 Analytical solution

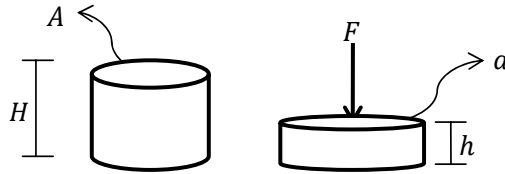


Figure 4.2: *Uniaxial compression of a cylindrical rubber. The true (Cauchy) stress is given by  $\sigma = \frac{F}{a}$  with  $a = \frac{A}{\lambda}$  due to incompressibility.*

The nominal stress  $F/A$ , which is defined as the force per original cross section area, can be obtained from the general strain energy density function of the Yeoh model [17]. This nominal stress is given by the following equation:

$$\frac{F}{A} = \frac{dW}{d\lambda} \quad (4.1)$$

Where  $W$  is the strain energy function of the Yeoh model given by the equation (3.10) as a function of the first strain invariants, and  $\lambda = h/H$  is the stretch, which gives a measure of the deformation.

In order to compare the results from the FE-simulation and the analytical solution it is necessary to have the equation of the nominal stress as a function of the stretches.

In a shock test only compression and stretch take place. The tension and compression deformation mode can be described as:

$$x = \lambda X \quad (4.2.a)$$

$$y = \mu Y \quad (4.2.b)$$

$$Z = \mu Z \quad (4.2.c)$$

The deformation gradient, given by the equation (3.3.b), and obtained from this deformation mode is:

$$\mathbf{F} = \begin{bmatrix} \lambda & 0 & 0 \\ 0 & \mu & 0 \\ 0 & 0 & \mu \end{bmatrix} \quad (4.3)$$

Using this equation and the fact that the principal stretches are obtained from the determinant of the left Cauchy-Greens deformation tensor  $\mathbf{B} = \mathbf{F}\mathbf{F}^T$ , it is possible to get the first strain invariant as follows:

$$I_1 = 2\mu + \lambda \quad (4.4)$$

Due to incompressibility:

$$\lambda_1 \lambda_2 \lambda_3 = 1 \rightarrow \mu^2 = 1/\lambda \quad (4.5)$$

$$I_1 = 2/\lambda + \lambda^2 \quad (4.6)$$

Using the equation (4.6) and the equation of the strain energy density function of the Yeoh model as a function of the first strain invariant, see equation (3.10), it is possible to get the strain energy function as a function of the stretches for this case of deformation:

$$W(\lambda) = C_{10} \left( \frac{2}{\lambda} + \lambda^2 - 3 \right) + C_{20} \left( \frac{2}{\lambda} + \lambda^2 - 3 \right)^2 + C_{30} \left( \frac{2}{\lambda} + \lambda^2 - 3 \right)^3 \quad (4.7)$$

Finally, the use of the equations (4.1) and (4.7) gives the nominal stress as a function of the stretches:

$$F/A = 2 \left( \lambda - \frac{1}{\lambda^2} \right) \left( C_{10} + 2C_{20} \left( \frac{2}{\lambda} + \lambda^2 - 3 \right) + 3C_{30} \left( \frac{2}{\lambda} + \lambda^2 - 3 \right)^2 \right) \quad (4.8)$$

This final expression of the nominal stress related to the original area was used to get the analytical solution of a uniaxial compression of a simple cylindrical model of the rubber. The maximum deformation of the cylinder in every loading case ( $h_{max}$ ) of the FE-simulation was used as an input in the equation (4.8) in order to get at the force in the moment of maximum compression of the system, see figure 4.5.

## 4.2 Estimation of the shear modulus $G$ using the Yeoh model and an energy balance

The main purpose of this section is to get an estimation of the possible shear modulus that may have the rubber with a hardness 52 shore A. In order to achieve this, the following two configurations have to be considered, see figure 4.3.

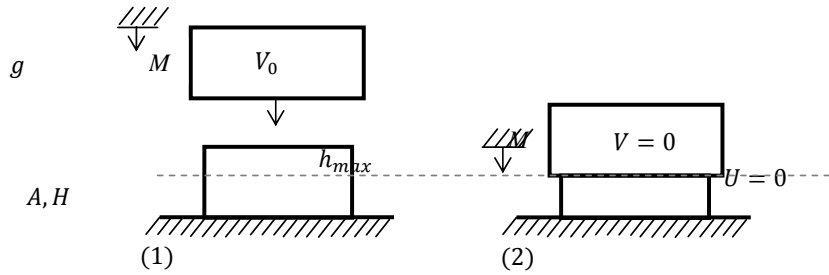


Figure 4.3: Configuration (1): initial state of the system; configuration (2): moment of maximum deformation of the rubber.

In the Yeoh material model, the strain energy density function  $W$  per unit of volume and as a function of the stretches  $\lambda$  is given by the equation (4.7). For the studied case, the stretch  $\lambda$  is given as the relation between the initial height ( $H$ ) and the height of the cylinder in the moment of maximum deformation ( $h_{max}$ ):  $\lambda = h_{max}/H$ .

Recalling the equation of the strain energy density function:

$$W(\lambda) = C_{10} \left( \frac{2}{\lambda} + \lambda^2 - 3 \right) + C_{20} \left( \frac{2}{\lambda} + \lambda^2 - 3 \right)^2 + C_{30} \left( \frac{2}{\lambda} + \lambda^2 - 3 \right)^3 \quad (4.9)$$

If the approximation of the rubber material parameters as a function of the shear modulus  $G$  is used, equation (4.11), the following linear equation for the strain energy function is obtained:

$$W(\lambda) = G \left[ \frac{1}{2} \left( \frac{2}{\lambda} + \lambda^2 - 3 \right) - \frac{1}{20} \left( \frac{2}{\lambda} + \lambda^2 - 3 \right)^2 + \frac{1}{200} \left( \frac{2}{\lambda} + \lambda^2 - 3 \right)^3 \right] \quad (4.10)$$

If an energy balance is done between the state (1) and the state (2), see figure 4.3, the following relation can be obtained:

$$T_{(1)} = T_{(2)} \quad (4.11)$$

Where  $T_{(1)}$  and  $T_{(2)}$  are the energy of the system in the initial state and in the moment of maximum compression of the rubber.

The energy in the state (1) is given by the following equation:

$$T_{(1)} = \frac{1}{2}MV_0^2 + Mgh_{max} \quad (4.12)$$

Where the first term correspond to the kinetic energy and the second term to the potential energy.

The energy in the state (2) is only internal energy ( $V = 0$ ) and is given by the strain energy density function multiplied by the volume of the cylinder:

$$T_{(2)} = A.H.W(\lambda) \quad (4.13)$$

The following equation can be obtained using the equation (4.13) and (4.10):

$$T_{(2)} = A.H.G \left[ \frac{1}{2} \left( \frac{2}{\lambda} + \lambda^2 - 3 \right) - \frac{1}{20} \left( \frac{2}{\lambda} + \lambda^2 - 3 \right)^2 + \frac{1}{200} \left( \frac{2}{\lambda} + \lambda^2 - 3 \right)^3 \right] \quad (4.14)$$

The following general equation is obtained inserting the equations (4.12) and (4.14) into the equation (4.11):

$$\frac{\left[ \frac{1}{2}MV_0^2 + Mgh_{max} \right]}{A.H} = G \left[ \frac{1}{2} \left( \frac{2}{\lambda} + \lambda^2 - 3 \right) - \frac{1}{20} \left( \frac{2}{\lambda} + \lambda^2 - 3 \right)^2 + \frac{1}{200} \left( \frac{2}{\lambda} + \lambda^2 - 3 \right)^3 \right] \quad (4.15)$$

Where the only unknown variable is the shear modulus  $G$ .

Finally, the equation (3.15) was used to get the estimation of the shear modulus  $G$ . In order to achieve this, the same values of maximum deformation that were obtained from the FE-simulation have been used. The figure 3.6 shows the linear function obtained from the equation (3.15) and the  $G$  value estimated.

### 4.3 Results

The figure 4.4 shows the graphic of the displacement and the force as a function of the time when the simple cylindrical rubber model is exposed to a impactor mass of  $M = 5 \text{ Kg}$  and initial velocity  $V_0 = 2 \text{ m/s}$ . Figure 4.5 illustrates the comparison between the force in the moment of maximum deformation of the rubber in the FE-simulation and from the analytical solution, for each loading case.

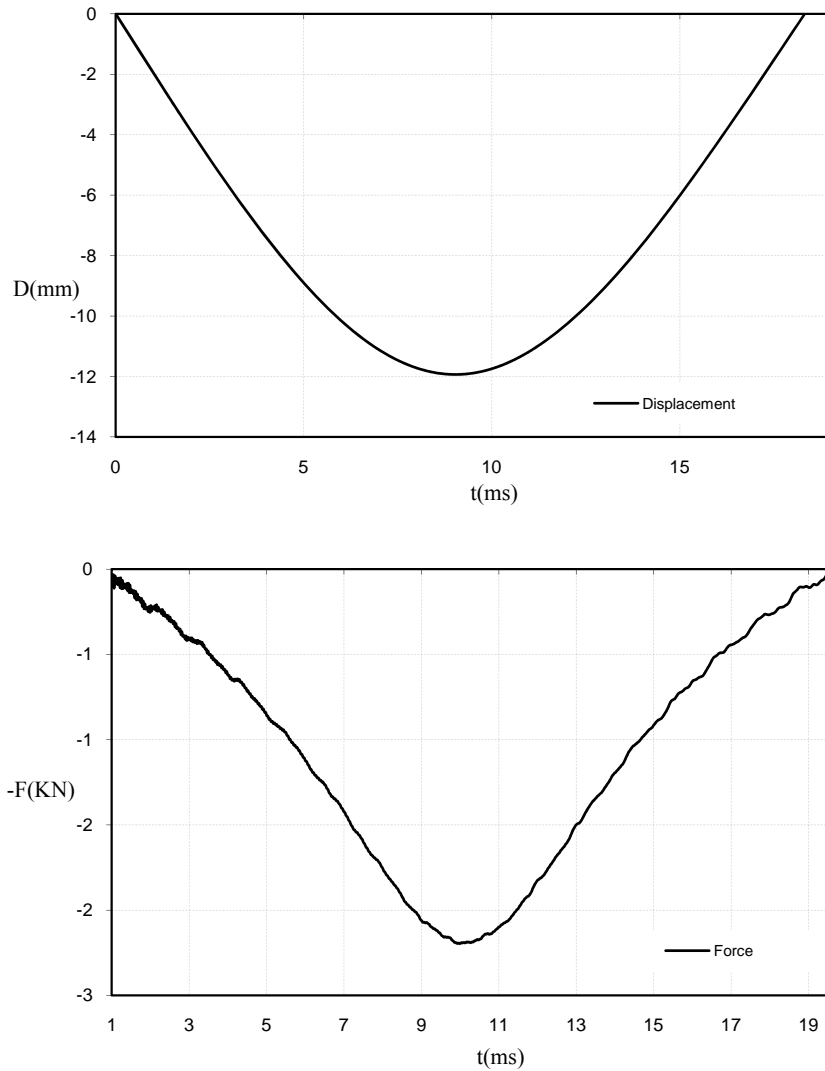


Figure 4.4: Displacement and force as a function of the time. Loading case:  $V_0 = 2$  m/s and  $M = 5$  Kg.

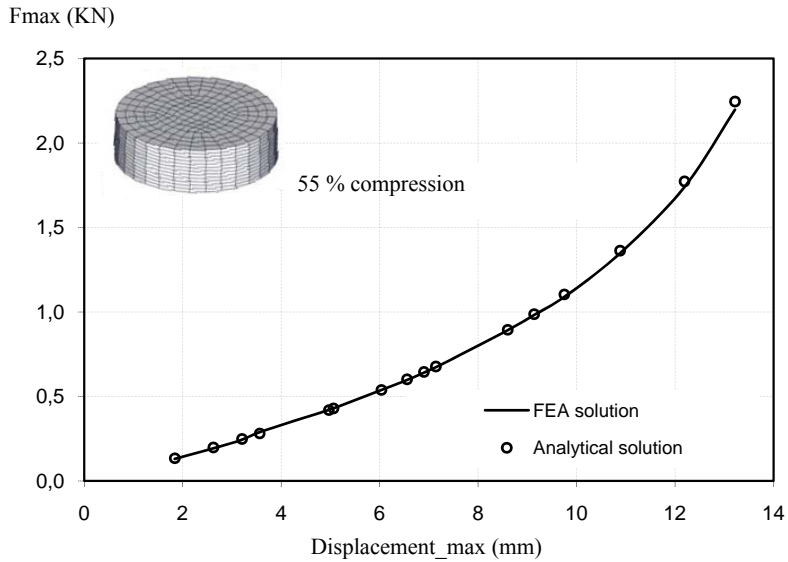


Figure 4.5: Comparison between the forces in the moment of maximum deformation of the rubber in the FE-simulation and from the analytical solution, for each loading case.

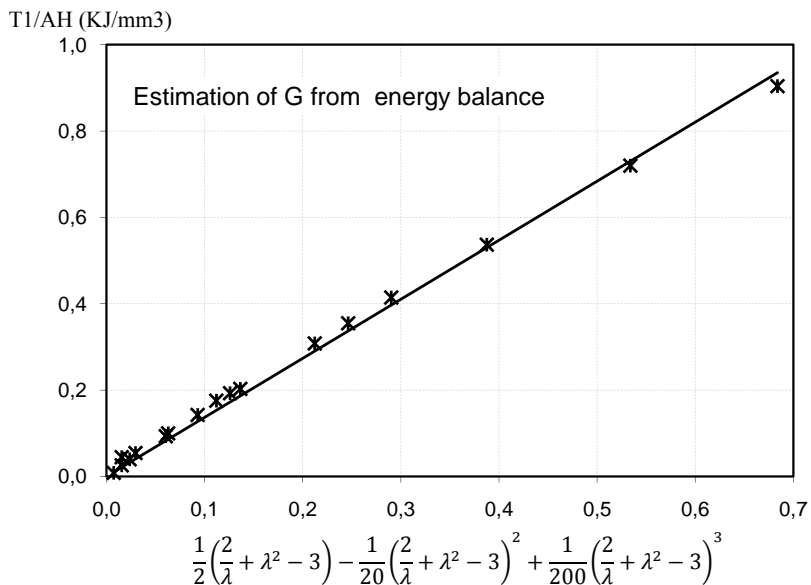


Figure 4.6: Estimation of the shear modulus  $G$  using an energy balance and the strain energy function of the Yeoh model, see the linear equation (4.15).

## 4.4 Analysis of the results

The maximum compression that could be obtained with the mesh of the simple model was around 55% of the initial height of the cylindrical rubber, see figure 4.4. If the model is compressed more than 55% of the height it starts having problems with negative volume, due to the small size of the elements (between 1 and 2 mm), and hourglassing. This is a phenomenon that appears in adjacent elements in hourglass-like formations and indicates that the results from the simulation are not reliable. This problem can be solved by increasing the size of the elements or changing the properties of the material. However, due to lack of time in this project it was not considered necessary improve the model in this simple analysis.

Figure 4.5 confirms that the results from the FE-simulation correspond quite well with the ones from the analytical solution when the Yeoh model is used as the hyperelastic rubber material to model the properties of the rubber.

The shear modulus  $G$  is given by the slope of the linear curve in figure 4.6 and is equal to  $G \cong 1,38 \text{ MPa}$ . The idea with this estimation was to get the shear modulus of the rubber with hardness 52 shore A. the balance energy method seems to give a good estimation of the value, since the shear modulus has to be approximately two times the value of the first material parameter  $C_{10} = 0,55$ . The difference between the values can be due to the rough estimation of the material parameters, since it was not possible to perform the experimental test in order to identify the rubber material parameters of the rubber.

# Chapter 5

## Development of FE model of the complete test setup of the rubber bushing system

Creating a FE-model of the rubber bushing that works effectively in the simulation of the full vehicle is the focus of this chapter. The complete FE model of the test setup has to be able to resemble, in as much detail as possible, the mechanical behavior of the rubber bushing. During a frontal car impact the rubber bushing is exposed mainly to a combination between shear forces, bending moments and axial forces. The complete test setup of the rubber bushing system is shown in figure 5.1. It is possible to note without any mathematical calculation that letting the drop weight fall close to the bolt head will result in the rubber bushing being exposed to more shear forces than bending moments and axial forces, but on the other hand, letting the drop weight fall away from the bolt head will cause exposure to axial forces and bending moments. For this reason and the facility available to build the experimental test setup, this configuration has been chosen to obtain experimental data and verify the final model.

The FE model of the test setup to perform the experimental tests of the rubber bushing mimics the real test setup that was built at the test rig of the Safety Centre of Volvo Car Corporation.

This chapter therefore describes the most important steps that have been taken into account while developing the finite element model of the complete test setup of the rubber bushing system, focusing on the rubber bushing itself. For more detailed information about the model the reader is referred to [1].

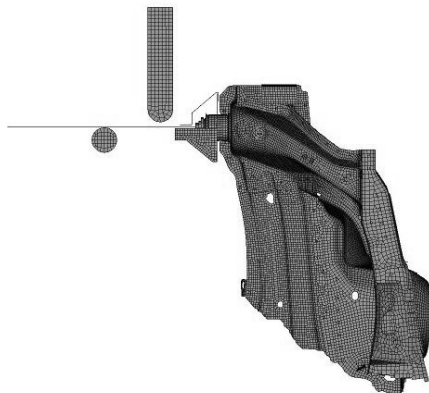


Figure 5.1: *Mesh of the complete test setup of the rubber bushing system.*

## 5.1 Development process of the FE-model and software implemented

This section briefly describes the fundamental steps of the development process that was used to create the final FE model of the rubber bushing.

The process of developing the finite element model of the complete test setup of the rubber bushing, with main focus on the rubber bushing itself, is shown in the figure 5.2.

The rubber bushing model has been developed starting from CAD 3-D geometry of the rubber bushing. Most of the geometry used to create the FE model has been created in the CAD design program CATIA V5.

The preprocessing part was carried out in two steps. The first preprocessing step while developing the FE model include the creation of an appropriate mesh for the model, the proper selection of material models and the assignment of material properties to the different parts of the model, and the definition of the parts that could come into contact with each other. These sub steps were carried out using ANSA after importing and converting the CAD geometries into ANSA files. ANSA is the advanced multidisciplinary CAE pre-processing tool that was used to create most of the FE model through the pre-processing decks of LS-DYNA, which is the multiphysics, explicit FE code used to solve the problem.

In order to properly describe the friction and contacts between the different parts of the complete rubber bushing system from the beginning of the simulation, the tightening of the bolt joint was taken into consideration. For that, an intermediate preprocessing step was carried out, which allowed achieving the deformed configuration of the rubber bushing system after the preload in the bolt joint and their initial strain and stress state.

To perform the intermediate preprocessing step the model obtained from the first step of the development process was saved with two different names: model 1 and model 2, respectively, as it is shown in the figure 5.2. One of these models was used to get the coordinates of the nodes of the deformed model and the initial stresses and strains of the elements, and the other was used to complete the preprocessing steps and get the final FE model.

The coordinates of the nodes and the initial stresses and strains of the elements due to the application of the preload in the screw joint were used as an input in the second preprocessing step.

All simulations must be driven by boundary conditions of some kind. In finite element analysis, these boundary conditions typically consist of forces, displacements or velocities that are applied to the model. This process of applying boundary conditions was also carried out in the second preprocessing step to finally get the final FE model.

After finally obtaining the FE model the postprocessing step of solving the problem begins. Two programs were used for this: LS-PrePost and Animator3.

LS-PrePost is an advanced interactive program for preparing input data for LS-DYNA and processing the results from LS-DYNA analyses. Animator3 is software used for visualization, animation and postprocessing for FEA. LS-PrePost was used mainly for XY plotting and Animator3 for 3D visualization and animation.

More information about each step of the process of the FE model development is described in more detailed in the next sections.

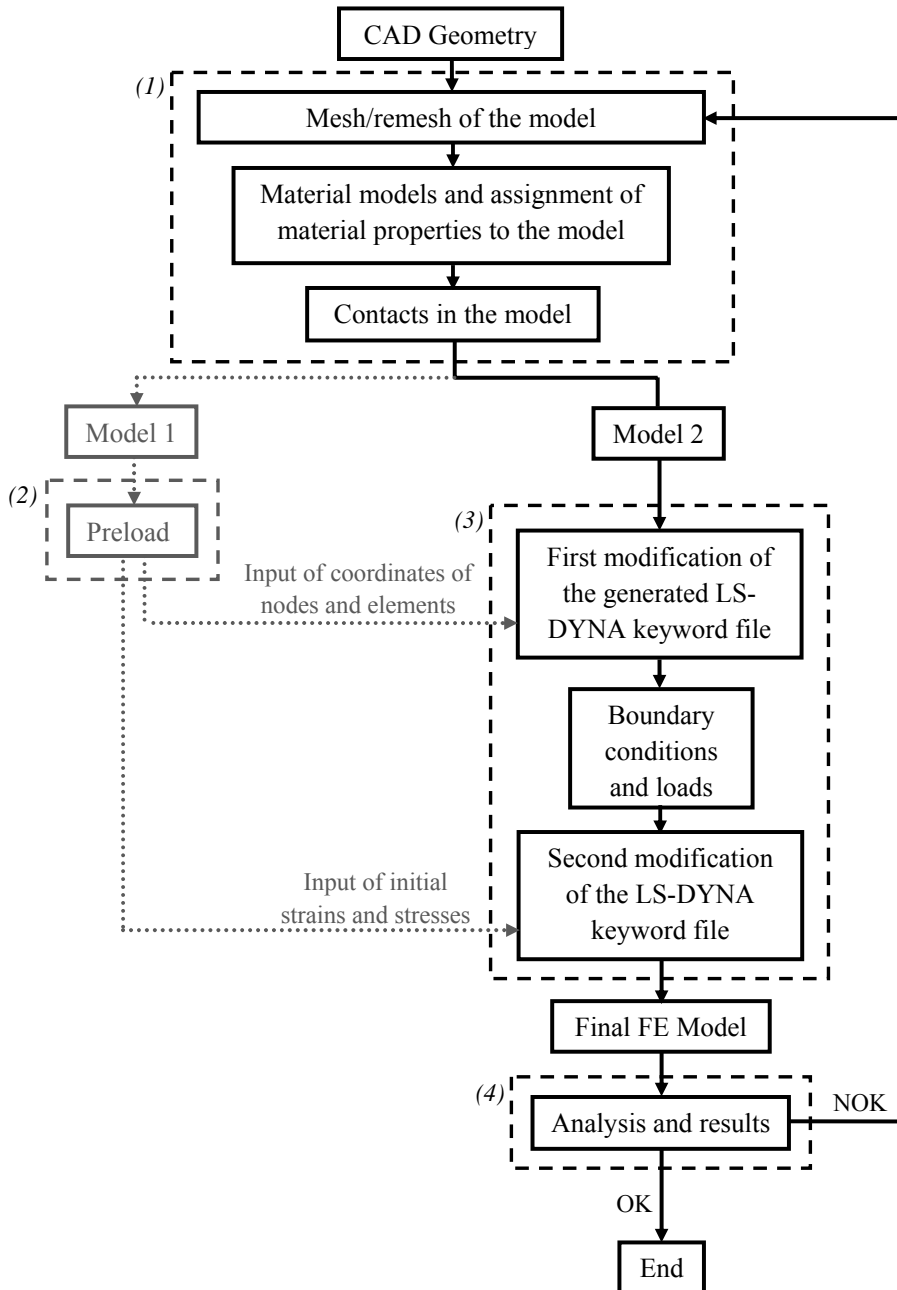


Figure 5.2: working scheme used to develop the FE model of the complete test setup of the rubber bushing system. (1): First preprocessing step; (2): Intermediate preprocessing step; (3): Second preprocessing step; (4): Postprocessing.

## 5.2 Geometry and mesh of the model

The mesh of the rubber bushing was generated from a CAD geometry, as it was explained in the section 5.1. The figure 5.3 shows the latest mesh created to model the rubber bushing. Due to the complexity of the geometry, some approximations and geometry clean-up had to be done to mesh the model as detailed as possible.

Despite of the fact that a fine mesh with a lot of elements gives more accurate results than a rough mesh, it was necessary to mesh the rubber part of the bushing in a rough way. This is because holes, fillets and other design features within the geometry of the rubber bushing rapidly increase the number of elements needed and, as a result, the computational cost of the analysis and the stability of the model are affected. Therefore, the smaller parts of rubber at the surface of the plastic outer sleeve, aluminum inner sleeve and at the corners while meshing the rubber bushing were not taken into account. These approximations in the rubber bushing had been therefore done considering that meshing process is time consuming and keeping in mind that the rubber mesh has to give a satisfying accuracy when testing the final model.

The rubber bushing was modeled using 8-node solid elements with 48 degrees of freedom and 4-node shell elements with 12 degrees of freedom. The 8-node solid elements were used for the rubber and the aluminum inner sleeve and the 4-node shell elements were used for the plastic outer sleeve.

The screw joint, which includes the bolt, the washer and the big nut, was modeled with 8-node solid elements, 4-node and 3-node shell elements and, 2-node beam elements with 6 degrees of freedom. The 8-node solid elements were used for the bolt head, the 2-node beam elements were used for the thread and the grip of the bolt, and the shell elements were used for the washer, the big nut and the cylindrical casing of the bolt.

Full integrated brick elements are the element formulation used for all the solid elements in the model. These formulations perform better when element distortions are large but are about four times more costly than in the case of one point integration [1]. On the other hand, the element formulation used for shell and beam elements were fully integrated shell element with Lobatto integration and Hughes-Liu beam with cross section integration, respectively.

The surrounding structures of the test setup model which include the drop weight, the sheet metal structure attached to the rubber bushing system and the support were modeled also with 4-node and 3-node shell elements, 8-node solid elements and 2-node beam elements. The 4-node and 3-node shell elements were used for the drop weight and the sheet metal structure attached to the rubber bushing system, the 8-node solid elements were used for the support and the 2-node beam elements were used to model the nut and the screw on the top of the impactor mass. The reason the screw and the nut on the top of the drop weight were modeled is to allow for the oscillatory movement of the drop weight while the screw bends. From this it is possible to mimic the real test setup and get more accurate results that can be compared with the data from the experimental test.

The drop weight and the support are assumed to be rigid bodies, due to the large difference in stiffness between these two parts and the rest of the model.

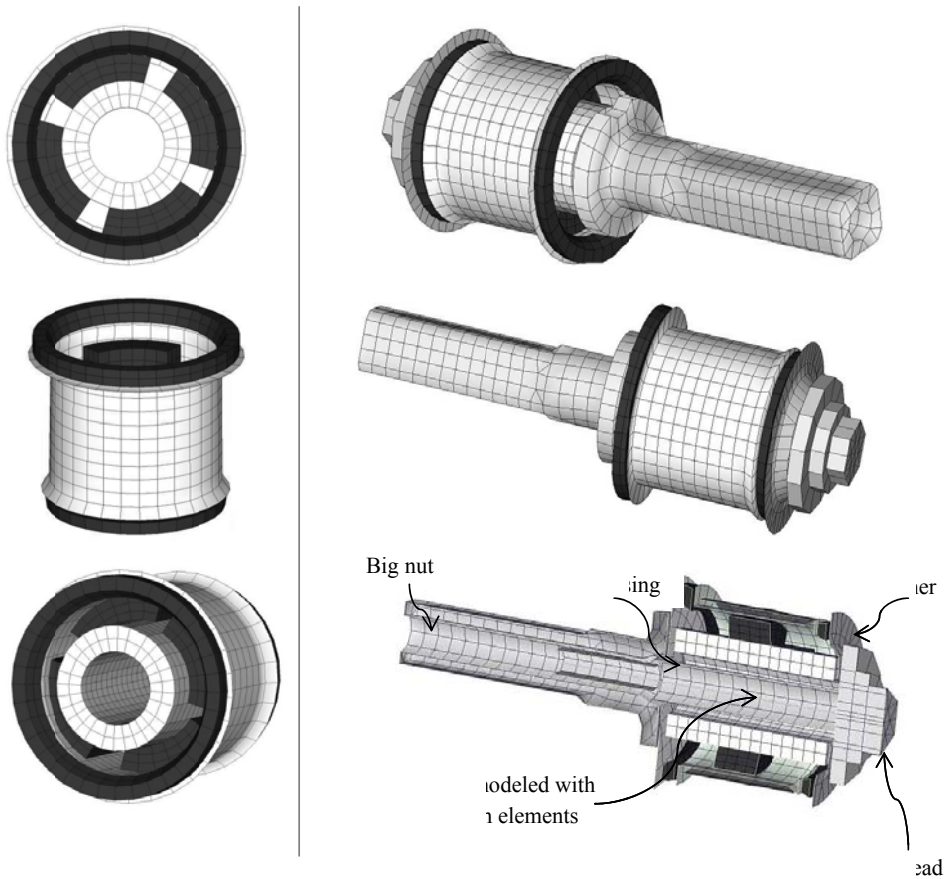


Figure 5.3: Left panel: Different views of the latest mesh of the rubber bushing: Top view of the rubber bushing (top), it is possible to see from this view the approximations at the corners of the rubber; side view of the bushing (middle); isometric view of the bushing (bottom). The side and isometric view show the part of rubber ignored at the surface of the outer and inner sleeve. Right panel: Different view of the rubber bushing with the components of the bolt joint.

### 5.3 Material models and assignment of material properties to the model

The complete model, as it is known, involves basically three materials, metal, plastic and rubber. Metal has a fairly linear stress-strain relationship at low strain values, but at higher strains the material yields and the response becomes non-linear and irreversible [7]. For plastic materials the response is also non-linear and irreversible even for low strain rate. Rubber is highly non-linear material and therefore the simple linear elastic stress-strain relation with a constant Young's modulus does not apply [7].

Hyper-elastic material model is used to model the rubber. In chapter 3, the general characteristic of the Yeoh model as a hyperelastic rubber material model were explained. In LS-DYNA, the general hyperviscoelastic rubber material type 77 was adapted for the Yeoh model. In order to achieve this adaptation, the constants  $C_{01}$ ,  $C_{11}$  and  $C_{02}$  were inputted as zero. Considering that it was not possible to carry out the experimental test in order to identify the rubber material parameter of the rubber, it was necessary to use a rough estimate of the material parameters using the value of the hardness in the rubber, which is 52 Shore A.

The value of the rough estimate of the hyper elastic rubber material parameters used in the final model are  $C_{10} = 0,55$  MPa,  $C_{20} = -0,05$  MPa and  $C_{30} = 0,95$  MPa. The mass density and Poisson's ratio were assumed to be  $\rho = 1,1 \cdot 10^{-6}$  Kg/mm<sup>3</sup> and  $\nu = 0,499$ .

For the rest of the FE model, the evaluated material models are mostly characterized by using elastic piecewise linear plasticity with a specific curve stress/strain and a yield strength.

### 5.4 Contacts in the model

Regarding the contacts in the complete rubber bushing system, the simple global contact was considered for almost all of the metal-metal surfaces. This allows a friction coefficient of 0,2. The contacts between the rubber and metals are complicated to model in an accurate way, since the rubber elements at the contact with other parts will be much distorted and they will penetrate the elements in the metal surfaces. This problem was solved by increasing the coefficient of friction to  $\mu = 0,8$ , which is the usual coefficient of friction between rubber and metal surfaces, and increasing the  $C_{30}$  parameter from 0,015 MPa to 0,95 MPa.

Contacts between the rubber and the plastic outer sleeve were solved by implementing the LS-DYNA option TIED\_NODES\_TO\_SURFACE\_OFFSET for tying the surfaces in contact with each other.

For contact between drop weight - sheet plate and support – sheet plate was used a coefficient of friction of 0,05 to simulate the condition of smooth surfaces and lubricated.

## 5.5 Preload

Preload has been taken into account while developing the FE model of the rubber bushing system. Despite of the fact that including the preload the modeling becomes more complicated, it was necessary to consider it, otherwise the model will not be as tight as it is in reality and will finally not be able to catch a behavior close to the real mechanical behavior of the system.

The preload, also called clamp force, is basically created when a torque is applied. During the tightening the bolt grip length is stretched, and the parts that are captured, which are the rubber bushing, the washer and the metal outer sleeve, are compressed. The result is similar to a spring-like assembly.

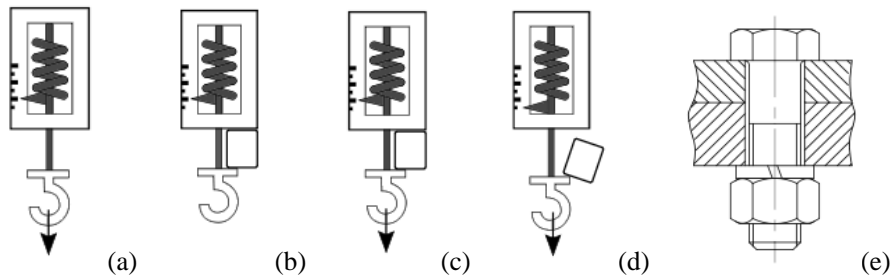


Figure 5.4: *Simplified model of a spring system. (a) Applying a preload of 1000 KN; (b) A block is inserted and the load is removed. The spring scale is unaffected; (c) any load may be applied, up to the preload, and the spring scale will not move, as long as the block is stiff; (d) only when the external load exceeds the preload does the spring scale move; (e) This analogy may be applied to bolt joints when the members being clamped are much more stiff than the bolt [19].*

The important role of the preload in the model can be roughly described making a comparison with the simple assembly of the spring, see figure 5.4. This means that a fully tightened bolt can survive in an application that an untightened, or loose bolt, would fail in a matter of seconds. In the case of the compressed member being less stiff than the bolt this analogy doesn't hold true. The load seen by the bolt is the preload plus the external load [19]. For this reason and the fact that the sliding force between two surfaces depends on the normal force that is applied on one of such surfaces, it was considered important to include the clamp load in the complete FE model of the rubber bushing system.

The clamp load after settlement in the complete rubber bushing system was therefore achieved under a quasi-static analysis ( $v = 0,24\text{mm/ms}$ ). A linear displacement was applied at the extreme of the bolt until it reached the clamp load, which was 84 KN. Boundary conditions were also considered for avoiding the motion of the big nut while applying the quasi-static displacement. For that, some of the internal nodes of the big nut were constrained with zero displacements in all directions.

## 5.6 Boundary conditions and loads

The boundary conditions are applied to avoid the motion of some parts of the model. Only five parts of the model are constrained: The support was constrained to avoid its movement in all the directions; the brace of the frontal subframe and the other part of the car chassis were constrained in three areas to simulate the fact that those areas are tight with screws; the other boundary condition was applied at one extreme of the beam elements located on the top of the drop weight, the beam was constrained with zero displacement on the node in all the directions, except for the vertical direction so the drop weight can fall.

In order to test the model different weights and initial velocities for the drop weight were applied. The mass of the drop weight was defined adding element mass to each node of the mesh of the drop weight. The initial velocity was applied on each node of the mesh of the drop weight and is given by the following equation:

$$V_0 = \sqrt{2 \cdot g \cdot H} \quad (5.1)$$

Where  $g$  and  $H$  are the gravity value, which was assumed to be  $9,81 \text{ m/s}^2$ , and the drop height, respectively.

# Chapter 6

## Laboratory experiments

The main purpose of the experimental tests was to get impact force curves between the drop weight and the sheet metal plate to verify the final finite element model in LS-DYNA. These tests were performed with different drop weights, drop heights and thicknesses of sheet metal plate in order to expose the system to different load cases. The rubber bushing was exposed to pulling out, bending moments and shear forces, as to reflect reality in the best possible way.

This chapter describes how the different tests of the test setup of the complete rubber bushing system were performed and their corresponding results. As a rule, the different tests will be appointed with their corresponding laboratory reference number. The FE-results corresponding to the different experimental tests are shown in chapter 7. In chapter 8 numerical and visual comparisons between the FE-simulations and the full-scale test will be made.

### 6.1 Equipment and test method

The tests have been carried out by the Test Engineer Stefan Skale at the test rig of the Safety Centre of Volvo Car Corporation. All tests have been performed with a vertical drop tower. The drop tower is capable of handling masses of up to 70 Kg and drop heights of 15 m.

Rubber bushing systems that will be used in the suspension system of Volvo cars are the study of this Master project. The Volvo X80-V70 front sub frame bushings used in this project have been manufactured and provided by Avon Automotive Company. The bushings are manufactured by injection molding the elastomeric material between outer and inner sleeve, vulcanizing and swaging. The inner metal sleeve is made of aluminum and the outer sleeve plastic. The elastomeric material is a carbon-black filled natural rubber of hardness 52 Shore A. The test specimen of the brace of the frontal sub frame was a cut out piece from the complete metallic sub frame of the frontal wheelhouse. The different metal sheets are manufactured by a forming process and are welded to each other. The screw joint, which keep the rubber bushing system linked to the sub frame of the wheelhouse is a M16 10.9 screw. The test setup of the complete system can be seen in figure 6.1.

The impact force between the drop weight and the sheet metal plate of the surrounding structure was measured using a force transducer located on the top of the drop weight, see figure 6.1. During the impact process the drop weight moved laterally. As a result of this problem, it was necessary to add beam elements on the top of the drop weight of the FE-model in order to mimic the lateral movement that the drop weight experience in reality. This fact should be kept in mind for further conclusions.

In order to make visual comparisons between full-scale and simulated tests, video is used to record the events. Two high speed cameras recording 1000 frames per second are placed in the test area in order to witness the complete and real time action. One of the cameras is set behind the drop tower to give a close view of the rubber bushing system. The other camera is placed in front of the drop tower to give a frontal view of the complete action. The process of data measurement and video acquisition starts at the exact time when the drop weight begins to fall.

Four impact tests have been planned to get experimental data. In the first test, reference number 09615701, the complete system was exposed to a drop weight of 40,085 Kg and initial drop height of 5,01 m, which was measured from the horizontal surface of the sheet metal plate. In test 09615702, a small sheet metal was welded and bolted to the surrounding of the structure, see figure 6.1. The thickness of the sheet metal plate and the height of the drop weight were also increased in order to get more bending moments and shearing force in the bolt joint and rubber bushing. The thickness of the sheet metal plate and the height were increased to 5 mm and 10,01 m, respectively. For test 09615703, the drop weight was increased to 55,285 Kg, the thickness of the sheet metal plate and the drop height were the same as in test 09615702. Due to the fact that one of the parts of the surrounding structure of the system was broken during the impact in the third test, it was necessary to reinforce the structure with welding and repeat the test in order to get reliable experimental data to verify the final FE model. Therefore, test 09615704 is the repetition of the third test with reinforcement in the structure. In test 09615704 a small metal cylinder with outer diameter of 25 mm and inner diameter of 24 mm was included to help reduce the lateral movement of the drop weight .A summary of the different impact tests carried out are shown in table 6.1.

Table 6.1: *Impact cases taking into account to get experimental data to verify the model.*

	Initial velocity (mm/ms)	Impactor mass (Kg)	Thickness of the plate (mm)
Test 1	9,905	40,085	4
Test 2	14,007	40,085	5
Test 3	14,007	55,285	5
Test 4	14,007	55,285	5

\* *The impact loads in the test 4 were exactly the same than the test 3 but the configuration of the system has some slight changes.*

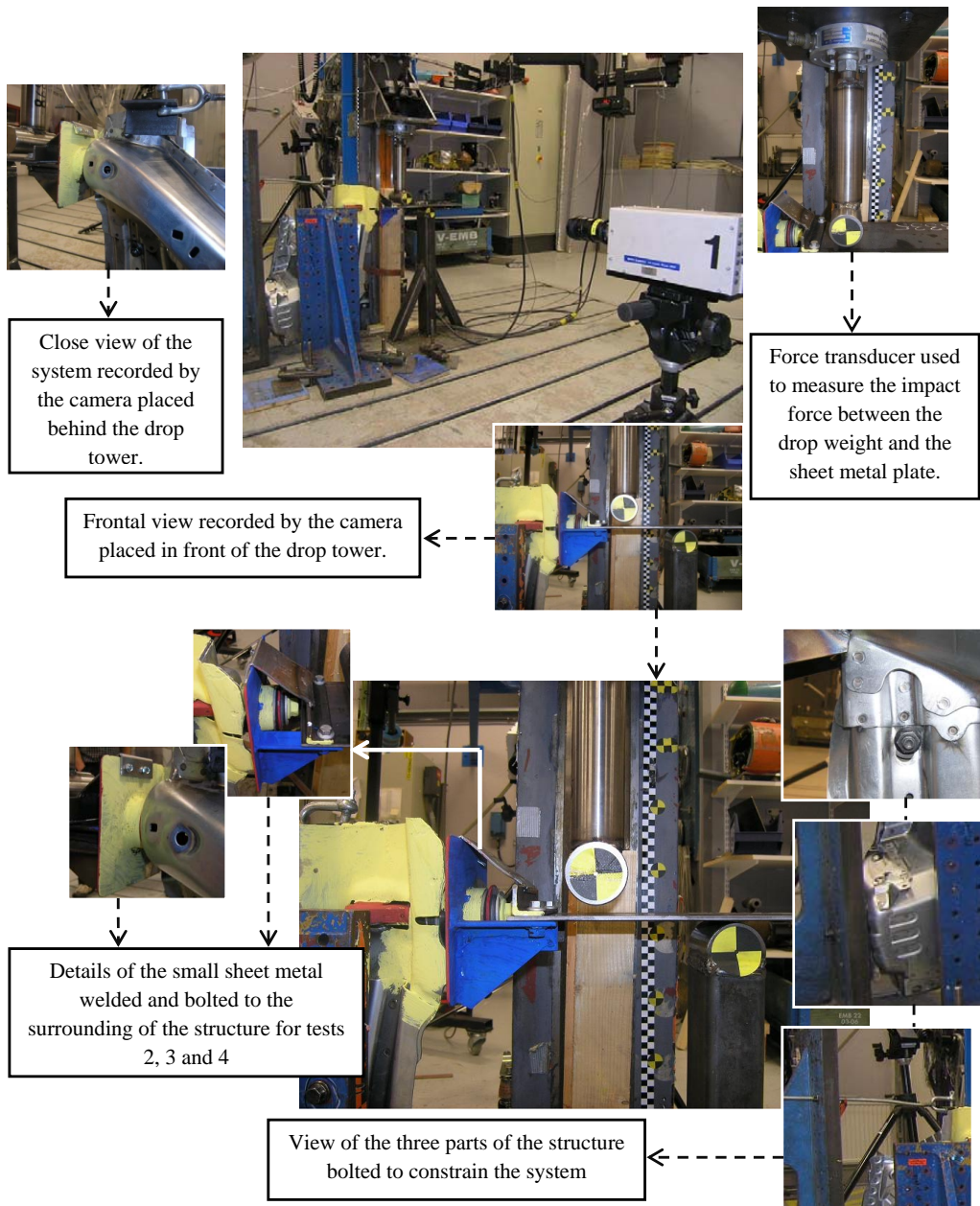


Figure 6.1: Test setup of the system showing the basic configuration to test the rubber bushing and get experimental data to verify the FE-model. Some other details are also shown and briefly explained.

## 6.2 Results

In this section the results for the experimental tests carried out at the test rig of the Safety Centre of Volvo Car Corporation are presented. Figures 6.3-6.4 shows the forces values obtained using the force transducer. 9600 data points were collected every  $6,25 \cdot 10^{-5}$  ms with 16-bit resolution.

In order to get a visual understanding of the different tests carried out some relevant pictures after the impact of tests 2 and 4 are shown in figure 6.2.

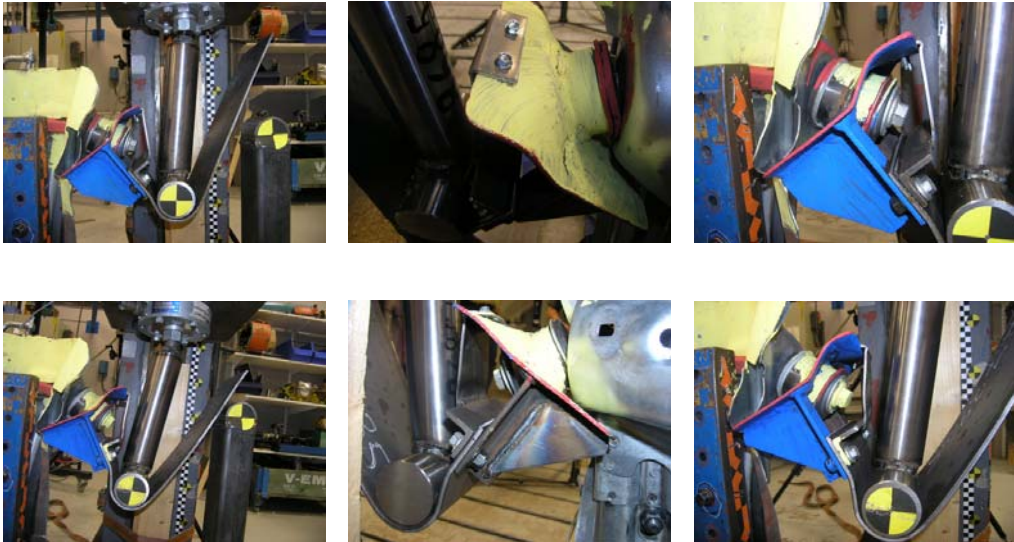


Figure 6.2: *Different views of the system after the impact. Upper part: test 2, lower part: test 4.*

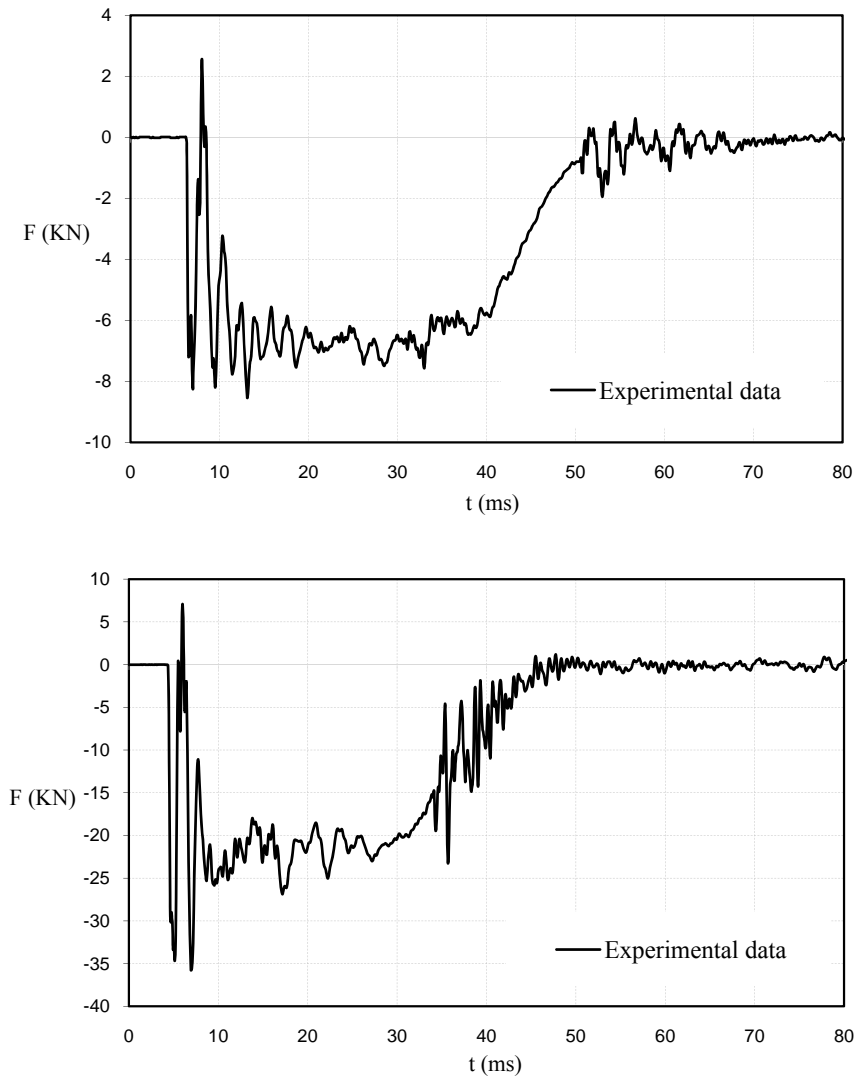


Figure 6.3: Impact force curves for experimental test 09615701 (top diagram), and 09615702 (bottom diagram).

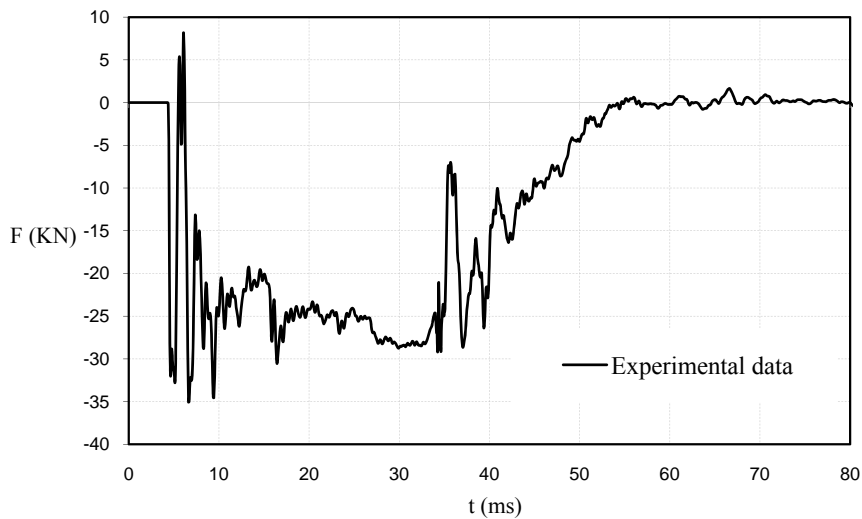
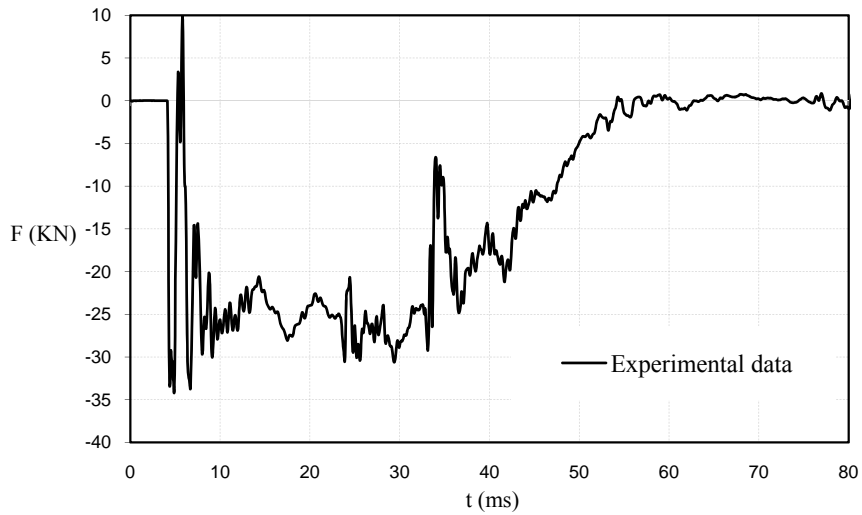


Figure 6.4: Impact force curves for experimental test 09615703 (top diagram), and 09615704 (bottom diagram).

# Chapter 7

## FE-simulations: Results and analysis

This chapter describes the results from the corresponding FE-simulations of the experimental tests. Afterward the results and where it is deemed appropriate, the different shock simulations made will be briefly discussed.

The forces values in the vertical direction of the drop weight have been considered to compare the output data from the FE-simulation with the experimental data from the full-scale test. The measurements from the FE-simulations have been taken at one extreme of the beam elements located on the top of the drop weight.

The configuration of the different simulated tests was explained in the previous chapter. Since the rubber material parameter  $C_{30}$  influences the behaviour of the rubber at high strain rate, different values have been used in the simulations in order to find out the rubber material parameter that ensures the stability of the simulation.

This chapter focuses on tests 2, 3 and 4, which are the significant tests performed to verify and validate the final model of the rubber bushing system. This is due to the fact that in these three tests it is possible to see the general mechanical behavior of the rubber bushing system.

## 7.1 Results

A cross-view showing the von Mises stress distribution that the rubber bushing system experiences during the different simulated tests carried out is shown in figures 7.1-7.4. Figures 7.5- 7.8 show the different graphs, obtained from the different simulated tests, for each rubber material parameter  $C_{30}$  tested.

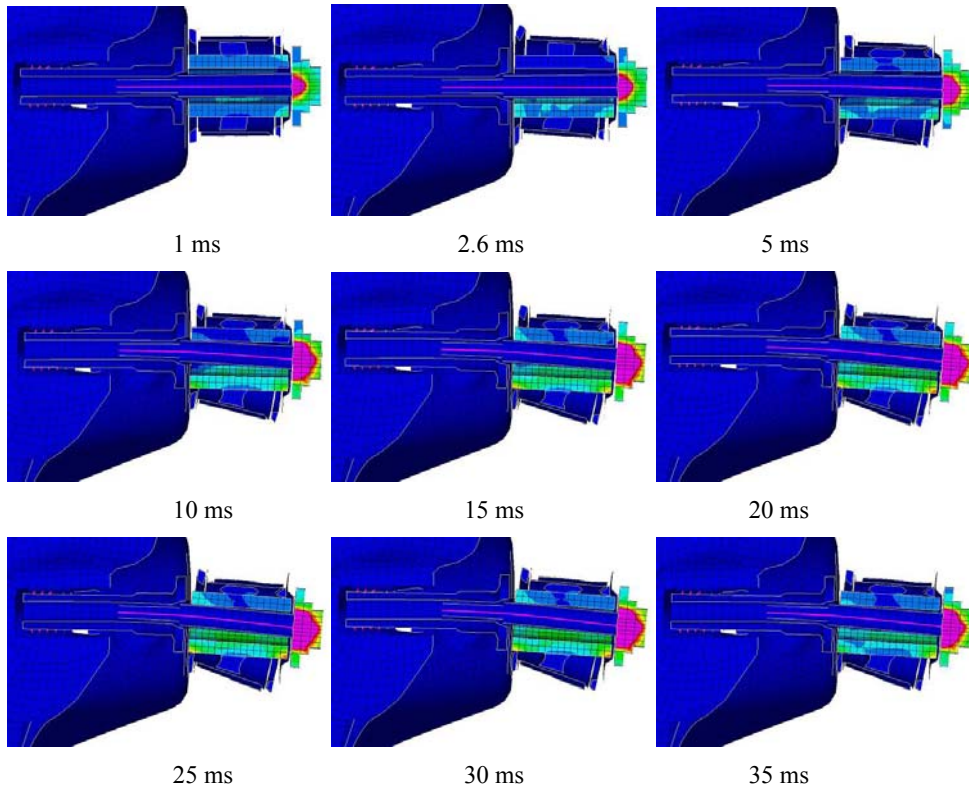


Figure 7.1: Time sequence showing the von Mises stress distribution that the rubber bushing system experiences during the first simulated test (corresponding to the experimental test 09615701).

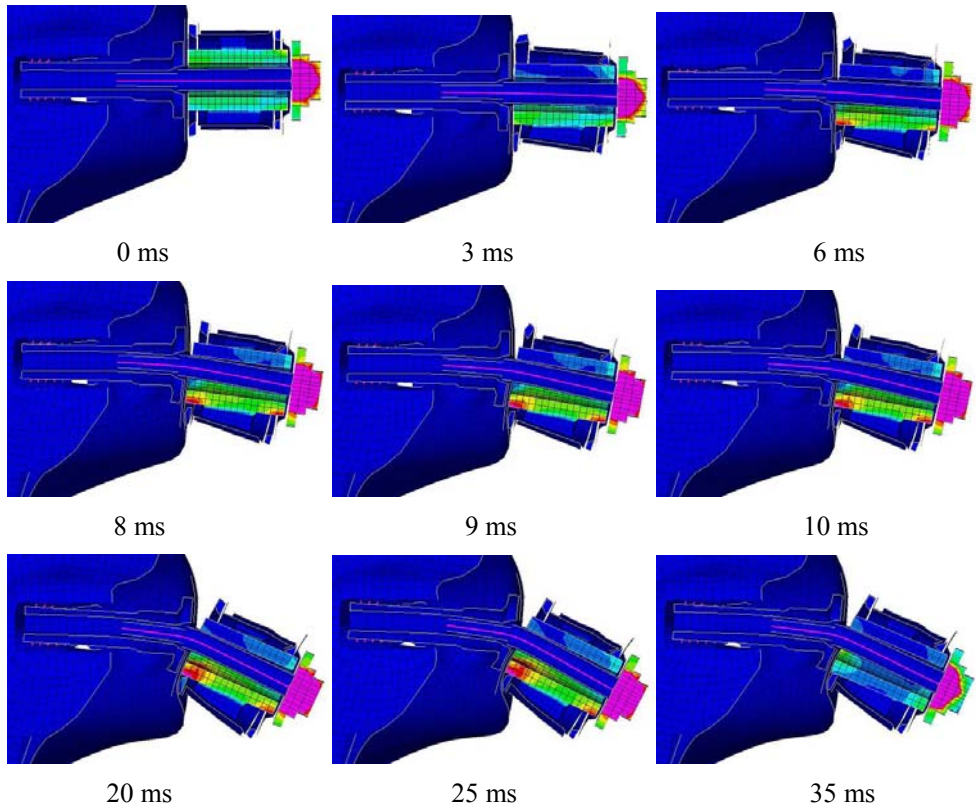


Figure 7.2: Time sequence showing the von Mises stress distribution that the rubber bushing system experiences during the second simulated test (corresponding to the experimental test 09615702).

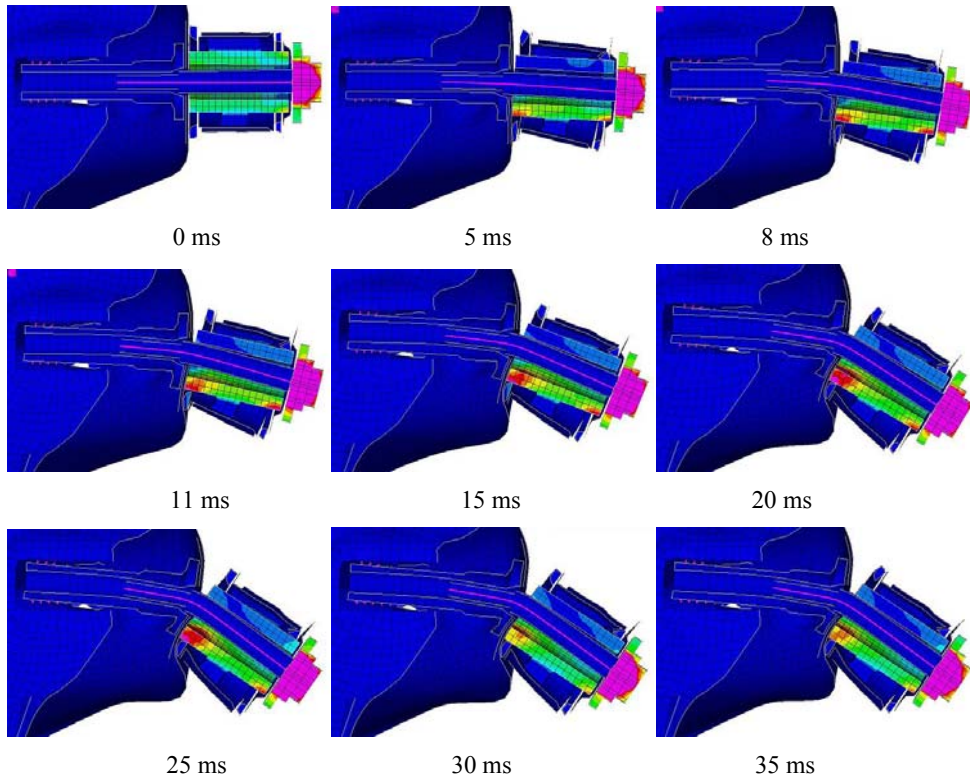


Figure 7.3: Time sequence showing the von Mises stress distribution that the rubber bushing system experiences during the third simulated test (corresponding to the experimental test 09615703).

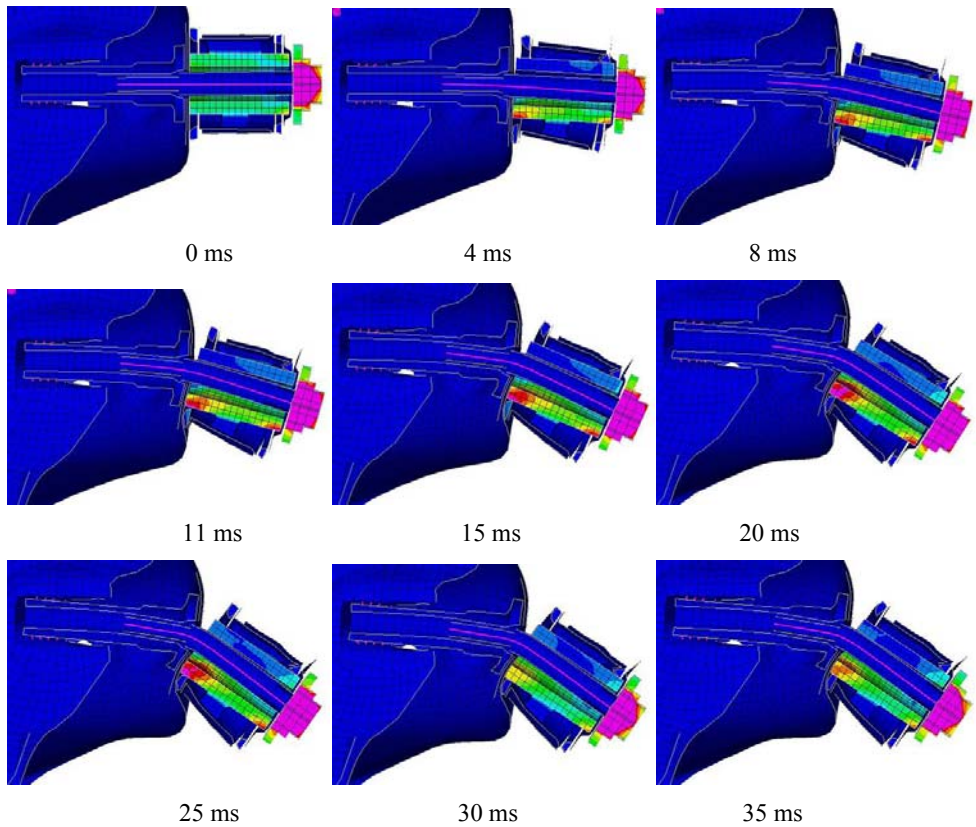


Figure 7.4: Time sequence showing the von Mises stress distribution that the rubber bushing system experiences during the fourth simulated test (corresponding to the experimental test 09615704).

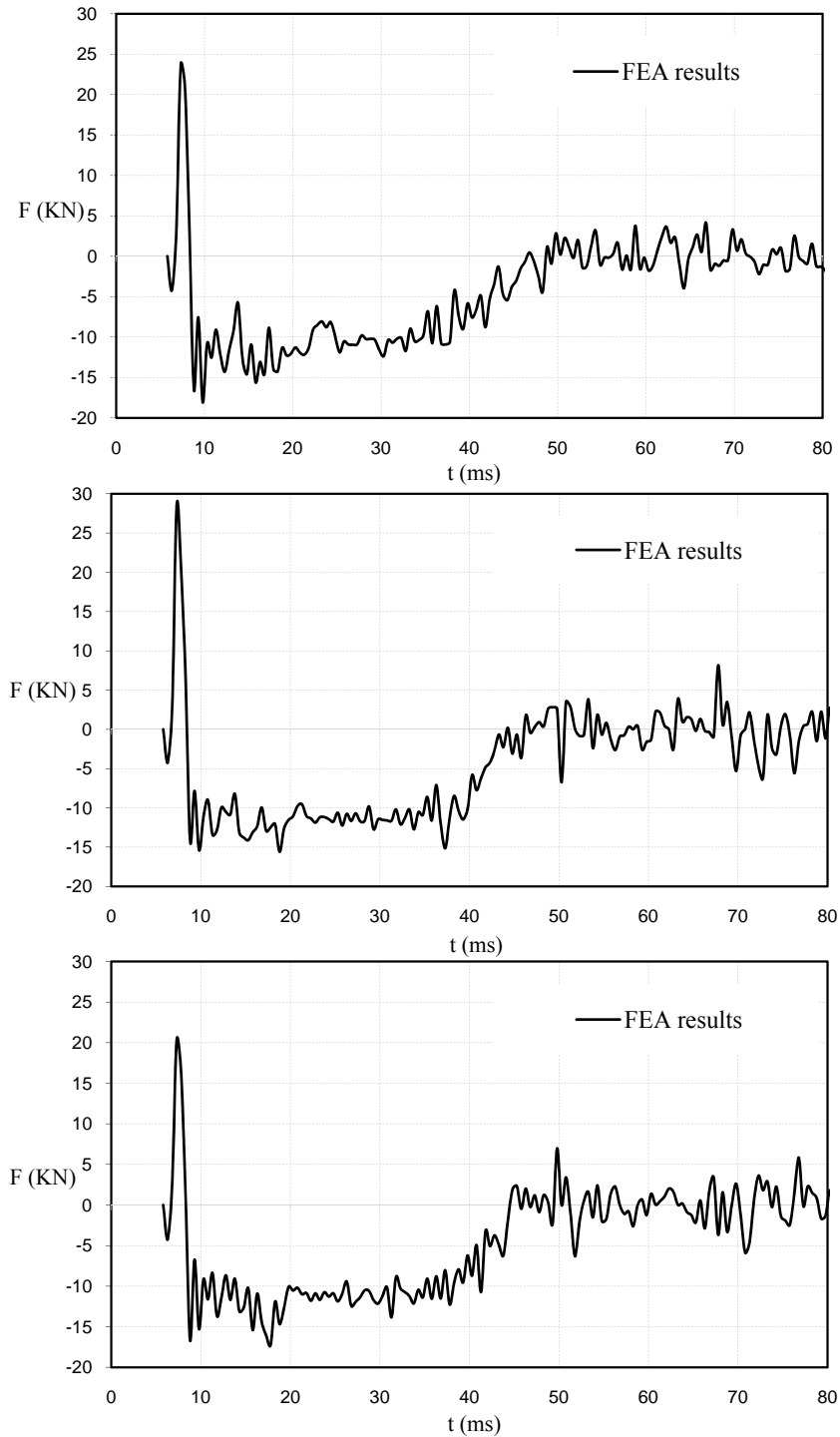


Figure 7.5: Force verification for the first simulated test using different rubber material parameter  $C_{30}$  in the FE model. Top-down:  $C_{30} = 0,25$  MPa,  $C_{30} = 0,55$  MPa and  $C_{30} = 0,95$  MPa.

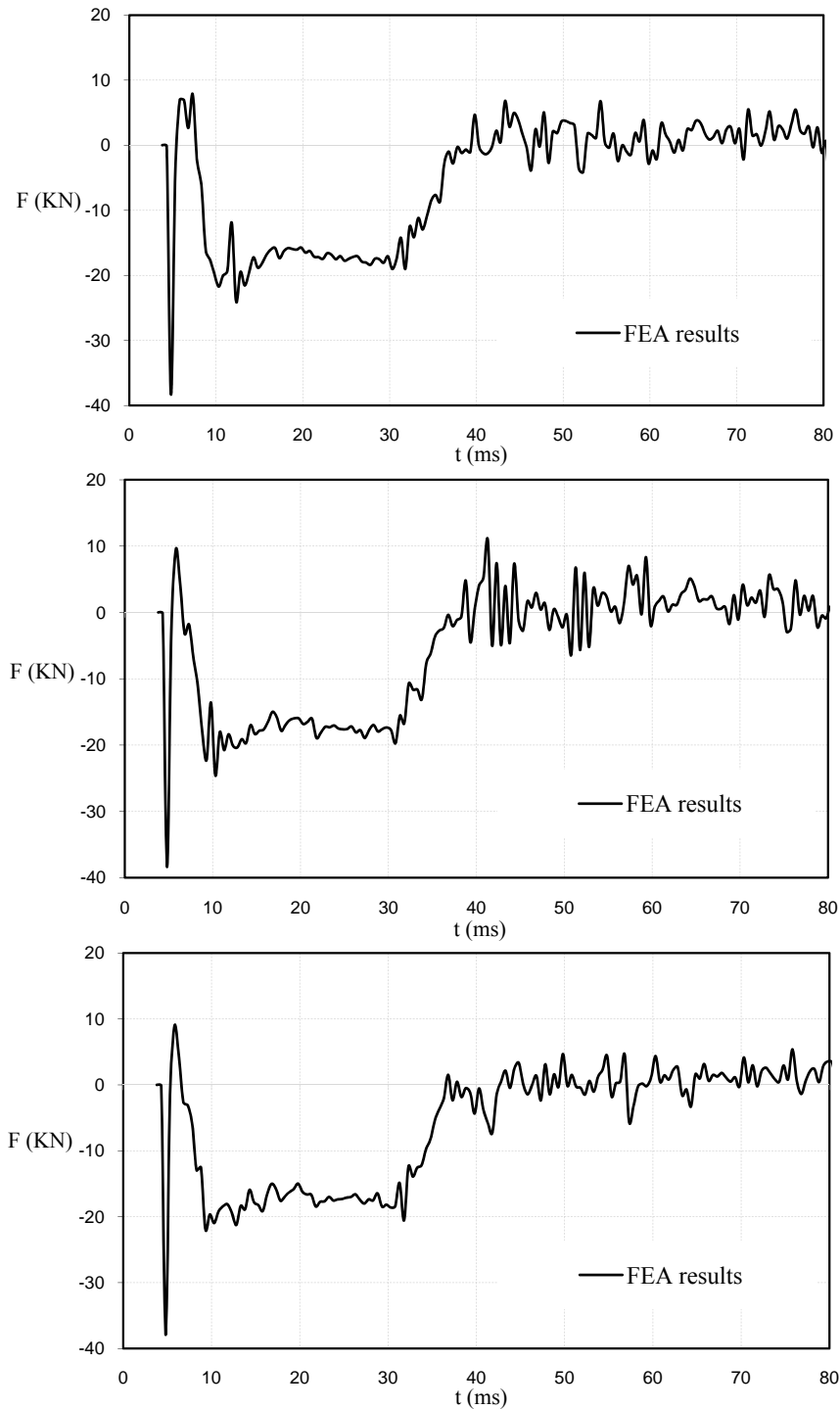


Figure 7.6: Force verification for the second simulated test using different rubber material parameter  $C_{30}$  in the FE model. Top-down:  $C_{30} = 0,25$  MPa,  $C_{30} = 0,55$  MPa and  $C_{30} = 0,95$  MPa.

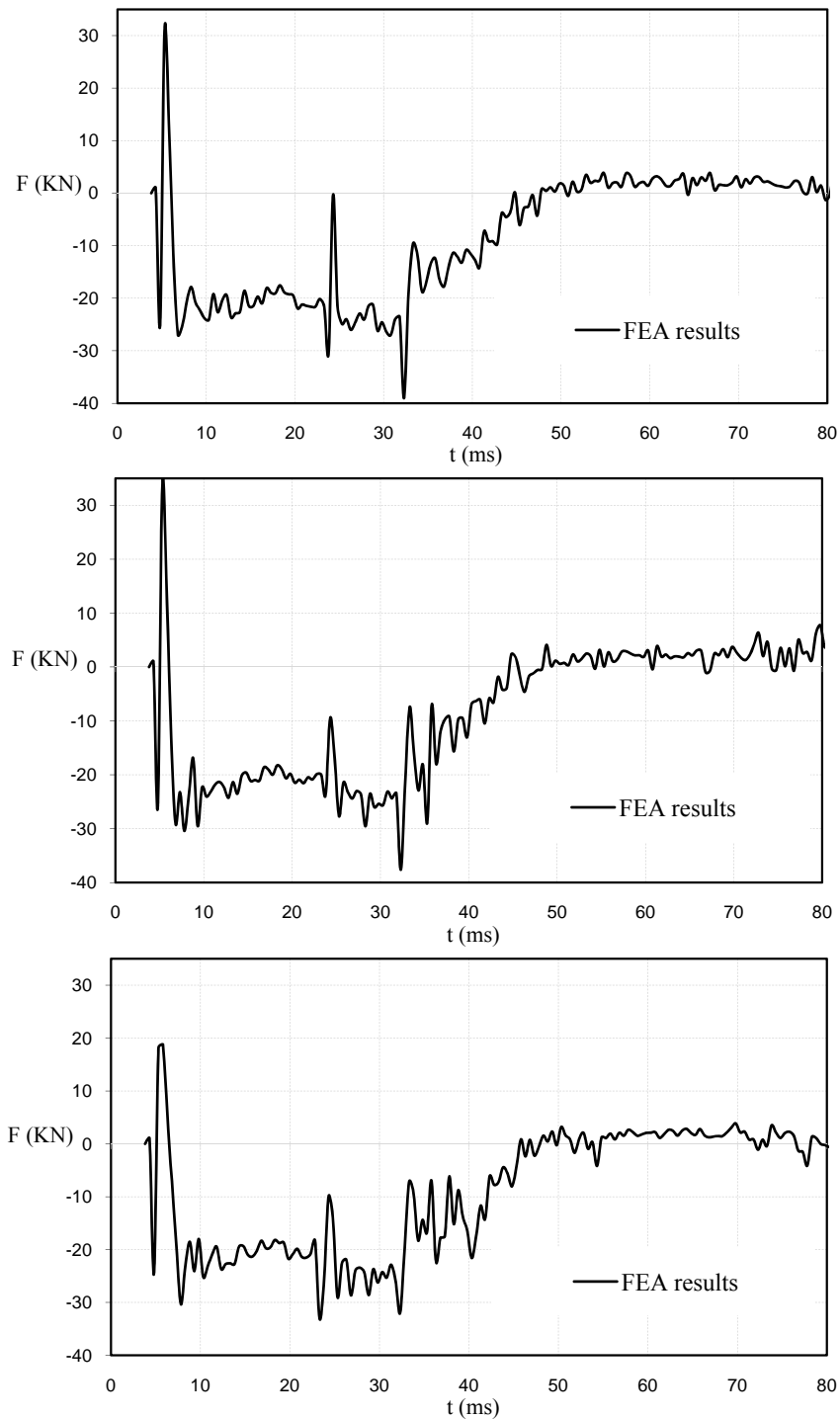


Figure 7.7: Force verification for the third simulated test using different rubber material parameter  $C_{30}$  in the FE model. Top-down:  $C_{30} = 0,25$  MPa,  $C_{30} = 0,55$  MPa and  $C_{30} = 0,95$  MPa.

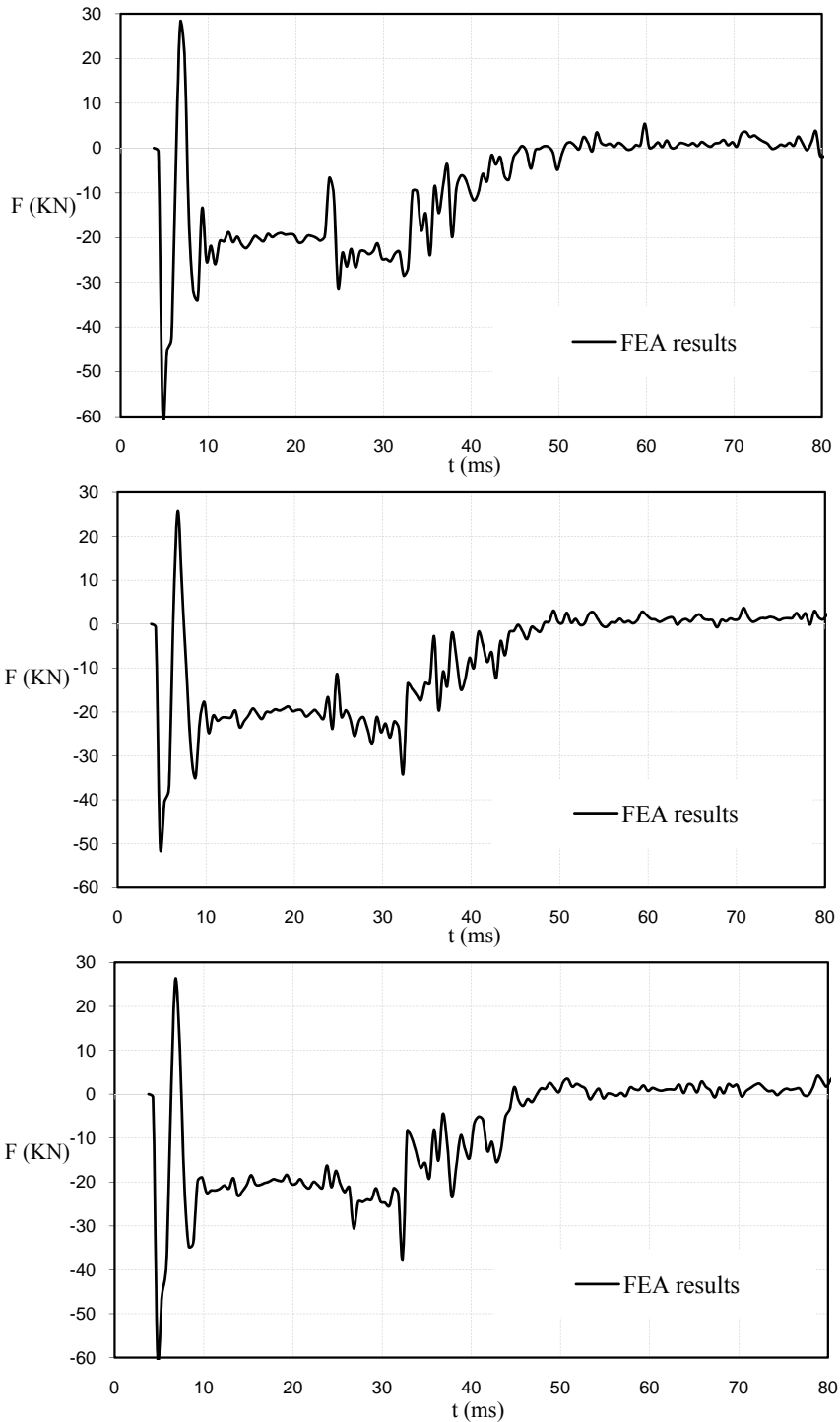


Figure 7.8: Force verification for the fourth simulated test using different rubber material parameter  $C_{30}$  in the FE model. Top-down:  $C_{30} = 0,25$  MPa,  $C_{30} = 0,55$  MPa and  $C_{30} = 0,95$  MPa.

## 7.2 Analysis of the results

During the first simulated test the rubber bushing system, including the bolt joint, deforms very little by the impact. It is only possible to see some radial compression in the rubber and pulling out between the metal and plastic outer sleeves, see figure 7.1. This is due to the fact that the sheet metal plate, which receives the shock loading, is too thin and absorbs most of the impact. Therefore, no further comparing between FE-simulations and the test 09615701 will be made.

In the second, third and fourth simulated tests, the small sheet metal welded to the surrounding of the structure added more bending to the screw joint. In figures 7.2-7.4 it is possible to see the considerable bending in the bolt joint and the pulling out between the metal and plastic outer sleeves.

Regarding tests 3 and 4, they are exactly the same test with the only difference being some parts of the surrounding structure of the complete system were reinforced with welding in test 4. The reason for this change was that some parts of the surrounding structure broke while performing the experimental test 3. The FE-simulation for both tests seems to be similar. Therefore, only the test 4 will be described in detail below.

Figures 7.2 and 7.4, the second and fourth simulated test, illustrate the immediate response of the rubber bushing system during the first 35 ms after the drop weight impact with the sheet metal plate. From these figures it is possible to note that the clamp force in the bolt joint starts working properly at the beginning of the FE-simulation. This means that the rubber bushing system, including the bolt joint, was highly tight from the beginning of the impact and the system does not deform very much in the axial direction, as it is supposed to be in reality. The friction in the system appears to be working properly during the simulation, since the aluminum inner sleeve appears to be stuck to the surface of the brace from the impact to about 7 ms for the second simulated test and 3 ms for the fourth simulated test. The aluminum inner sleeve starts sliding after the noted times. The bolt joint starts bending at about 8 ms in both tests and it keeps on bending until the drop weight lost contact with the sheet metal plate at about 30 ms and 38 ms for the second and fourth simulated test, respectively. Due to the difference of drop weight between the tests, it is possible to note that the bolt bends more in the tests 4 than in the test 2. It is also possible to see the pulling out effect in the system since the washer seems to be deformed a little. This is due to the relative movement between the metal outer sleeve and the plastic outer sleeve, which makes the metal outer sleeve compress the rubber lips and make them bend the washer.

Figures 7.5- 7.8 show the different graphs, obtained from the different simulated tests, for each rubber material parameter  $C_{30}$  tested, The graphics do not differ very much from each other, but the parameter  $C_{30}$  influences the stability in the system, since the rubber elements during the impact distort a lot and they penetrate the elements in the metal surfaces. The rubber material parameter that gave more stability and prevented penetration between elements in the system was  $C_{30} = 0,95$  MPa.

In summary, the FE-model seems to mimic, in a very good way, the general mechanical behavior of the rubber bushing system when it is exposed to high shock loadings. The preload in the bolt joint, the contacts and the friction between the surfaces work properly as well as the bending and pulling out behaviour of the system. Despite many approximations in the Yeoh model, it seems to be a good choice to model hyperelasticity in rubber-like materials.

# Chapter 8

## Validation

In order to validate the final FE-model of the rubber bushing system a numerical and visual comparison between the FE-simulations and the experimental test made at the test rig of the Safety Centre of Volvo Car Corporation, will be made.

The numerical comparison will be made by comparing the experimental data (impact force between the drop weight and the sheet metal plate), which was measured using a force transducer located on the top of the drop weight, and the FE-results. The force values in the complete FE-model of the test setup of the rubber bushing system were measured at one extreme of the beam elements located on the top of the drop weight.

For visual comparison high speed cameras were used together with visualizations and videos in AVI format obtained from Animator3.

Finally, in order to be sure that the final FE-model of the rubber bushing system works properly in the full-vehicle crash simulation an US-NCAP analysis has been performed in LS-DYNA. According to the U.S. National Highway Traffic Safety Administration (NHTSA), which is the company that began crash-testing popular vehicles models in the United States, The US-NCAP analysis is basically a full-width frontal impact collision where the vehicle crashes head-on into a rigid concrete barrier at 35 mph (56 Km/h) [18], see figure 8.1.

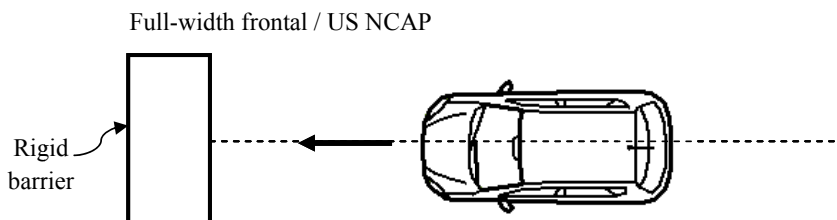


Figure 8.1: *Full-width frontal impact crash test.*

In order to carry out this last simulation, the complete rubber bushing system previously developed has been included in the right side of the frontal subframe of the full vehicle simulation. Due to lack of time the old bushings in the rear and left side of the complete car were not replaced by the new bushing. In the end, an evaluation of the impact and a comparison between the full vehicle crash simulations with the traditional FE-model of rubber bushing that often is used in the car and the new FE-model of rubber bushing system are made.

## 8.1 Results

Figures 8.2-8.4 show the visual comparison between the different full scale and simulated tests that have been performed at the test rig of the Safety Centre of Volvo Car Corporation and by using LS-DYNA, respectively. Figures 8.5-8.8 show the impact force history for the different simulated tests with rubber material parameter  $C_{30} = 0,95 \text{ MPa}$ , which was the value that was considered appropriate to simulate the final FE-model and guarantee the stability of the simulation. The plots for the experimental data are here just added with the FE-results.

Figures 8.9 and 8.10 show the times sequences for the full-vehicle crash simulation with the traditional and new FE-model of rubber bushing system.

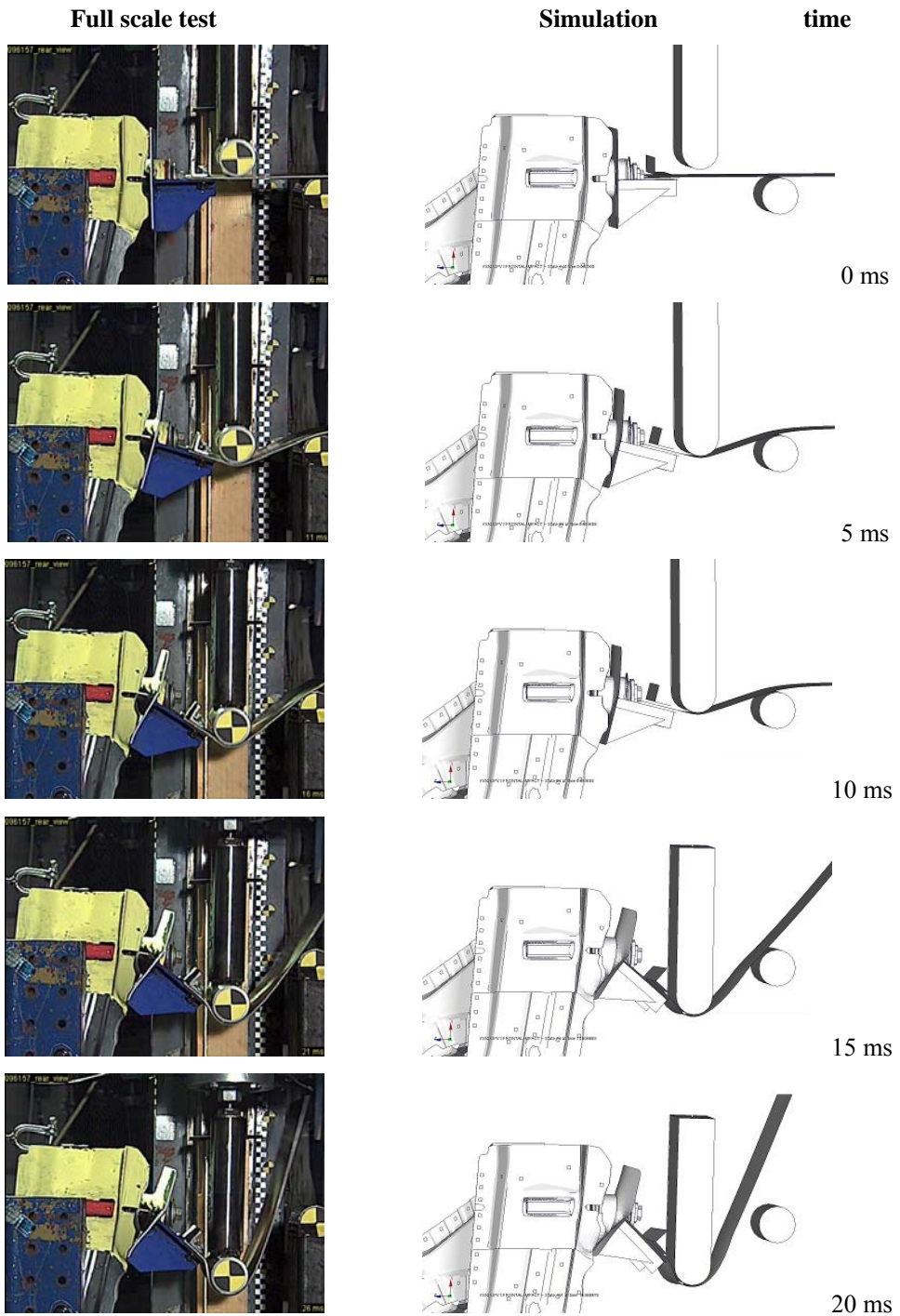


Figure 8.2: Comparison between first full scale and simulated test (initial height = 10,01 m, and drop weight = 40,085 Kg).

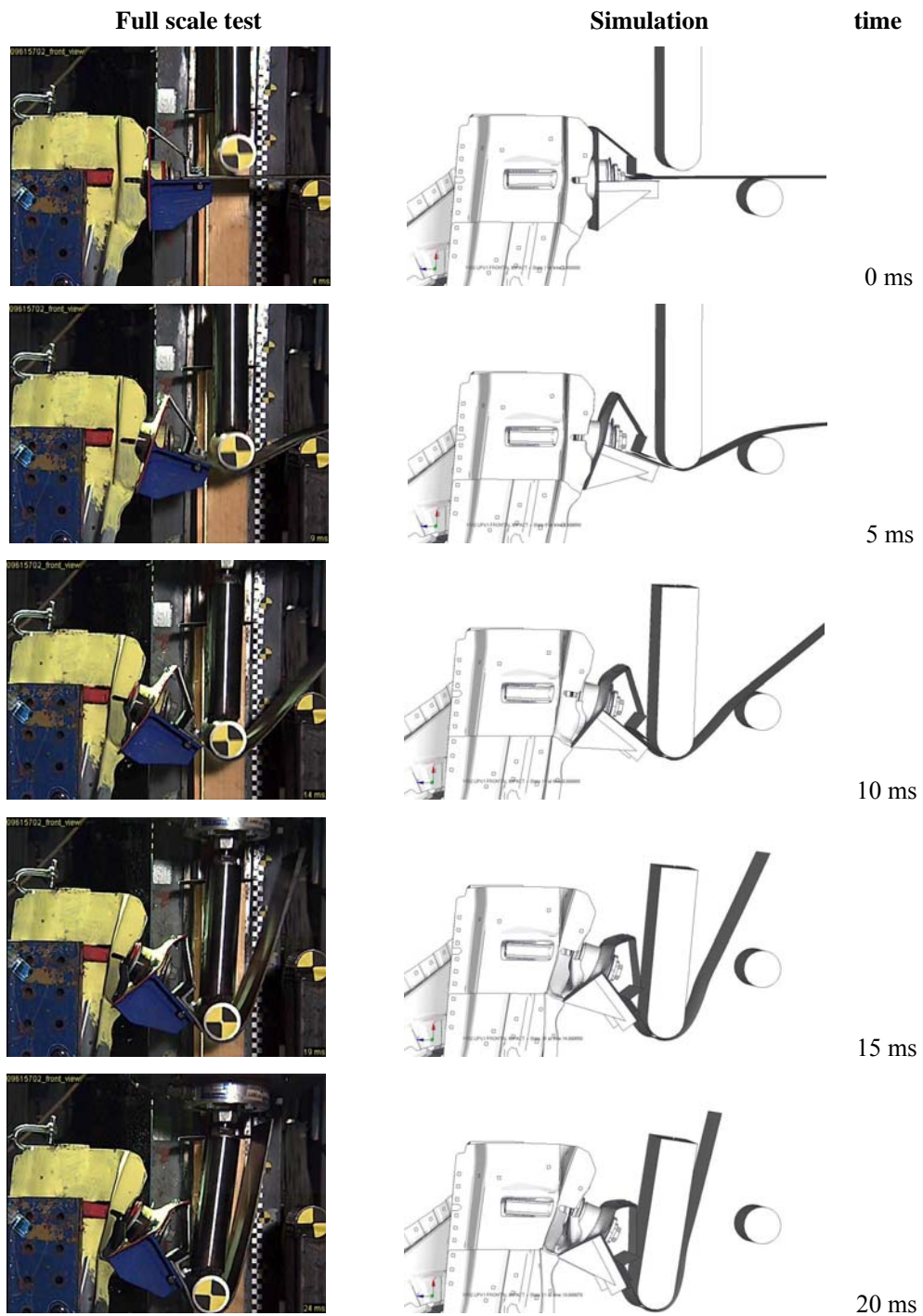


Figure 8.3: Comparison between second full scale and simulated test (initial height = 10,01 m, and drop weight = 40,085 Kg).

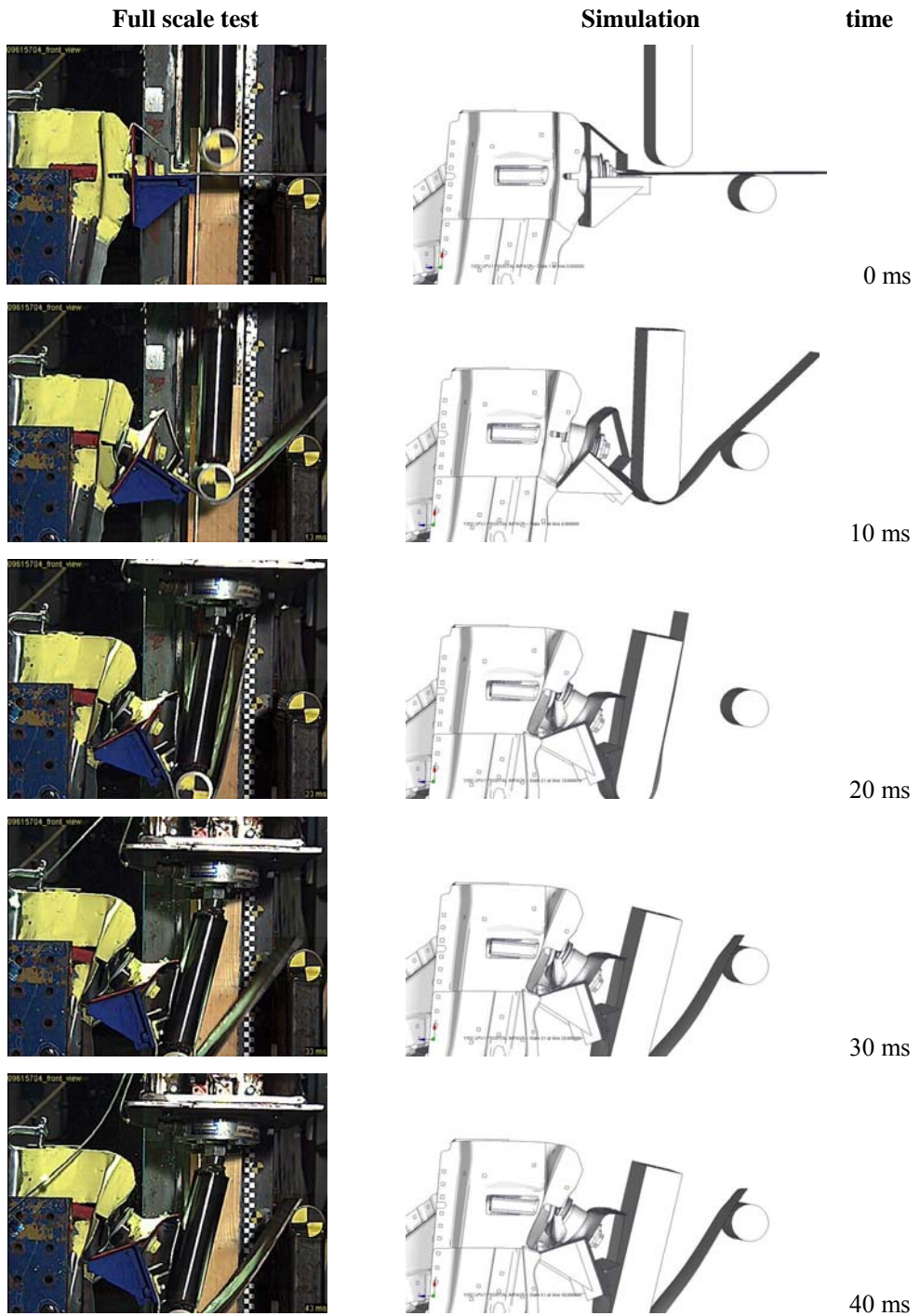


Figure 8.4: Comparison between fourth full scale and simulated test (initial height = 10,01 m, and drop weight = 55,285 Kg).

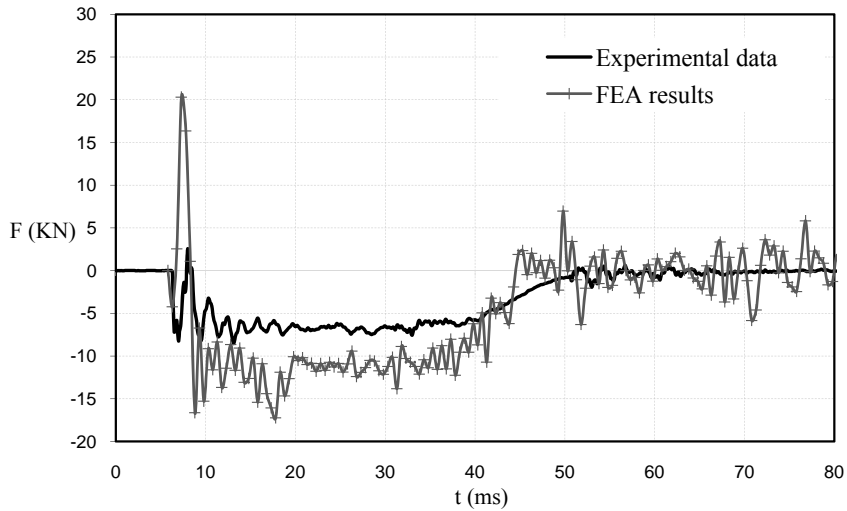


Figure 8.5: Validation of the FE model of rubber bushing by comparison of the impact force history of experimental data to FE-results for the first test. ( $C_{30} = 0,95 \text{ MPa}$ ).

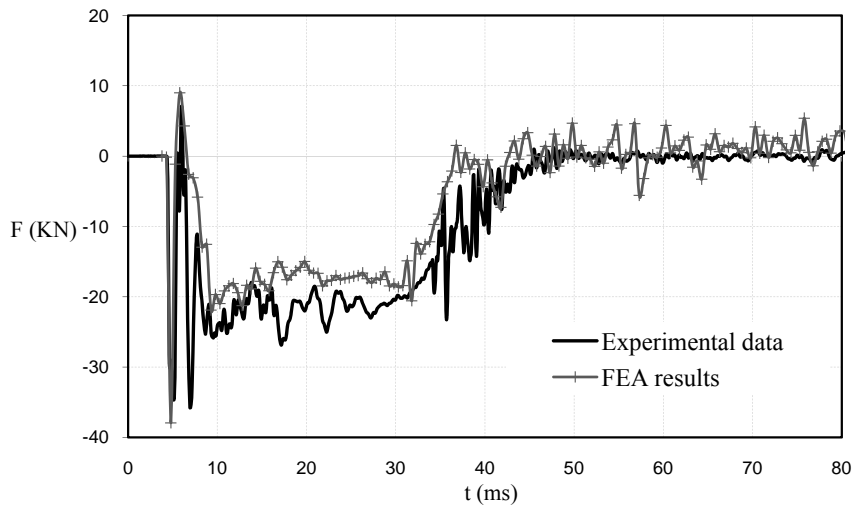


Figure 8.6: Validation of the FE model of rubber bushing by comparison of the impact force history of experimental data to FE-results for the second test. ( $C_{30} = 0,95 \text{ MPa}$ ).

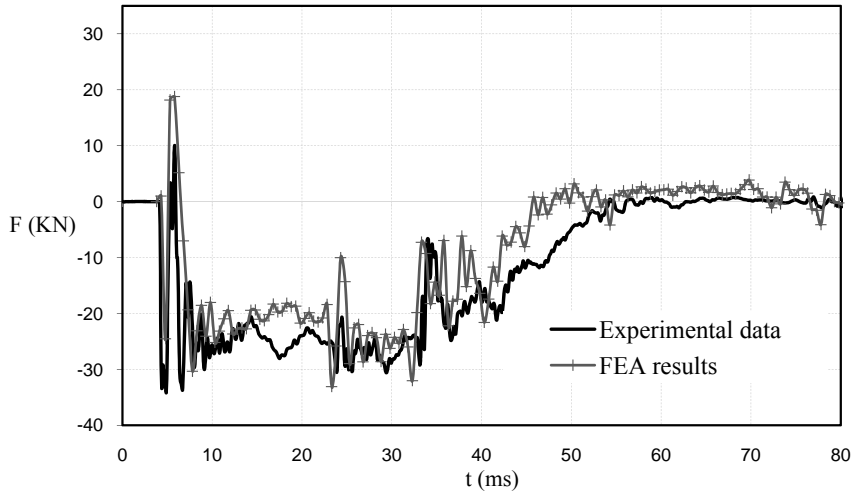


Figure 8.7: Validation of the FE model of rubber bushing by comparison of the impact force history of experimental data to FE-results for the third test. ( $C_{30} = 0,95 \text{ MPa.}$ ).

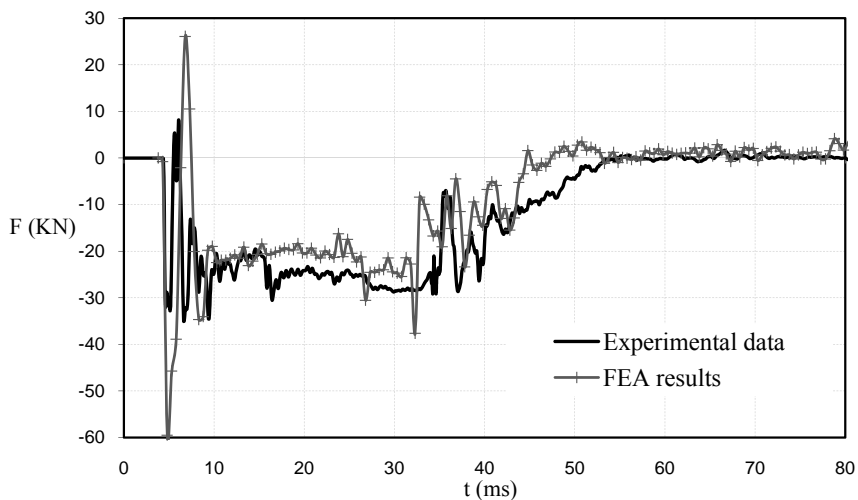


Figure 8.8: Validation of the FE model of rubber bushing by comparison of the impact force history of experimental data to FE-results for the fourth test. ( $C_{30} = 0,95 \text{ MPa.}$ ).

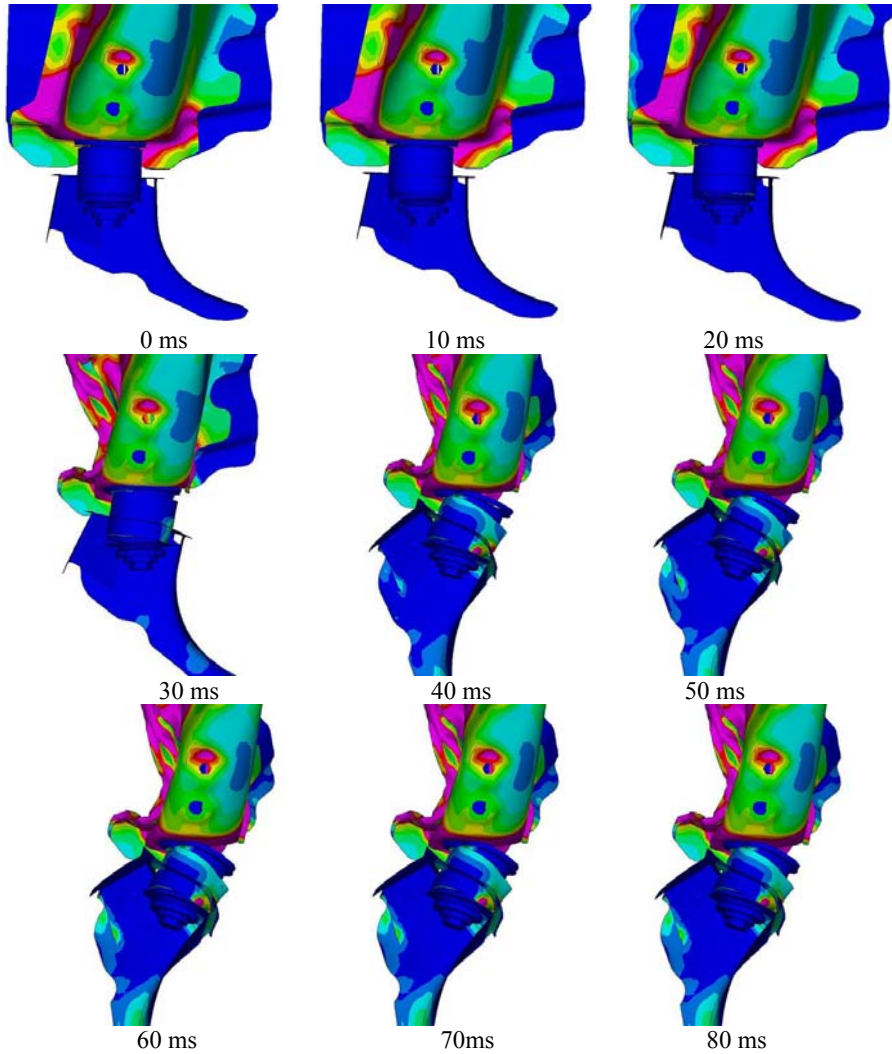


Figure 8.9: Time sequence from full-vehicle crash simulation (35 mph) with the new FE-model of rubber bushing system in the right side of the frontal subframe.

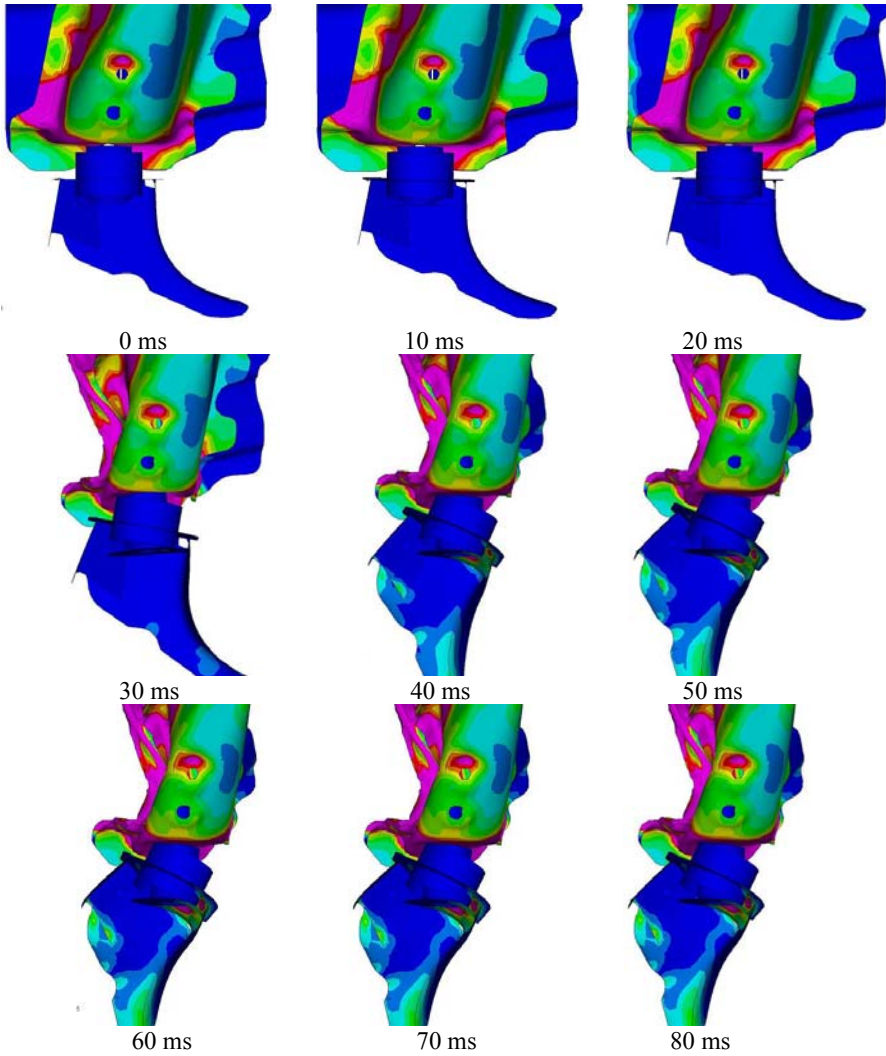


Figure 8.10: Time sequence from full-vehicle crash simulation (35 mph) with the traditional FE-model of rubber bushing system that often is used in the full-vehicle.

## 8.2 Analysis of the results

By looking at the chronologies shown in the figures 8.2-8.4, similarities between the different tests can be observed. Slight differences in the position of the system were noticed when comparing the recorded videos of the full-scale test with different visualization and videos in AVI format obtained from Animator3. The slight differences are due to the fact it was not possible to constrain some parts of the body sub frame in a good way, and as a result, the body, which is suppose to be static in the bolted areas, slides in the same direction of the drop weight (vertical direction).

Figures 8.5-8.8 plainly show the comparisons between the predicted resultant drop weight impact force history from the simulations and the ones measured from the different experiments, The simulated outputs and the experimental measurements agree qualitatively but they differ in magnitude. Such a difference is probably caused by many approximations in the geometry of the FE-model and, other source of error which include the measurements in the experimental test and many approximations in the hyperelastic rubber material model. Another possibility for the difference is that the complete test setup of the rubber bushing system does not exactly mimic the real test setup because it was not possible to constrain the body sub frame adequately.

Regarding the US-NCAP simulation of the full-vehicle with the new rubber bushing system, the model behaves very well in the simulation. The deformations of the rubber bushing system as a result of the bending moment, axial force and pulling out between sleeves appears to be similar to what happens in reality, see figure 8.9. In comparison, figure 8.10 shows the behavior of the traditional rubber bushing system in the full-vehicle crash simulation. In this case, it is not possible to see the complete behavior of a real rubber bushing system, since the model does not have a physical modeling with solid elements for the rubber and the bolt joint. This makes the traditional model of the bushing too simple to capture the real mechanical behavior that a rubber bushing system experience in reality.

Despite the fact that the new FE-model of rubber bushing is more complex than the traditional one, the elapsed time for the full-vehicle crash simulation was reduced by approximately 4 % when implemented in the full-vehicle (just in the right side of the frontal subframe). This result makes the final FE-model more suitable and desirable than the traditional one.

In summary, the full-scale impacts and computed deformations agree qualitatively but they differ in magnitude. The differences can be caused by many approximations in the FE-model and others source of error while carrying out the different experimental tests. However, the model can be considered reliable and can be used with a high rate of confidence.

# Chapter 9

## Conclusions

This Master's thesis project focused on developing and validating a new and improved finite element modeling of rubber bushing for crash simulations.

The rubber itself is just a small part of the complete rubber bushing system, so it was not necessary to use a complex material model to predict the physical response of the rubber. A simple and purely hyperelastic rubber material model where no damping exists was used instead. The Yeoh model worked out to be a stable model at high strain rate and therefore was used with these material parameters:  $C_{10} = 0,55$ ,  $C_{20} = -0,05$ ,  $C_{30} = 0,95$ .

The developed FE-model of rubber bushing system seems to model the nonlinearities in the system as large displacement effects and large deformations, material nonlinearity, and boundary nonlinearities. This is confirmed by the preload in the bolt joint, the contacts, the friction between the different surfaces and the bending and pulling out behaviour of the system working properly at the beginning and during the simulation.

In order to validate the final FE-model of the rubber bushing system it was exposed to different loading cases in the FE-simulations and full-scale tests. The FE-simulations were tested under the same conditions as in the experimental tests in order to have a reference for comparisons. The full-scale impacts and computed deformations agreed qualitatively but they differed in magnitude. The deformations of the rubber bushing system, due to the bending moment, axial force and pulling out between sleeves appear to be similar to what happens in reality. The reason for the inaccuracies may be caused by several approximations in the FE-model and others source of error while carrying out the different experimental test.

An US-NCAP analysis was also performed in LS-DYNA in order to be sure that the final FE-model of the rubber bushing system works properly in the full-vehicle crash simulation. The simulation provided satisfactory results in the full-frontal impact of the car showing a significant improvement in the behavior of the rubber bushing system in comparison with the full-vehicle crash simulation of the traditional FE-model of rubber bushing that is often used in the car.

Finally, the final FE-model of rubber bushing system can be considered reliable and can be used with a high rate of confidence in the full-vehicle crash simulation, since the computational time can be reduced by up to 4 % approximately and when used in the full vehicle crash simulation, this model is more physical and detailed than the traditional one and can better resemble the mechanical behaviour of the real rubber bushing system.



# References

- [1] *LS-DYNA Theory manual Version 971*, Livermore Software Technology Corporation, 2006.
- [2] Hibbitt, Karlsson and Sorensen, *ABAQUS/Standard User's Manual Version 5.8*, 1998.
- [3] Krenk S., *Non-Linear Modelling and Analysis of Solids and Structures*, 2008.
- [4] Belytschko T., Liu W.K. and Moran B., *Nonlinear Finite Elements for Continua and Structures*. Wiley, Chichester, U.K. 2000.
- [5] Cook R.D., Malkus D.S. and Plesha M.E., *Concepts and Applications of Finite Element Analysis*. John Wiley & Sons, 1989.
- [6] Ottosen N.S. and Ristinmaa M., *The Mechanics of Constitutive Modeling*, Elsevier, 2005.
- [7] Johansson B. and Järhage O., *Verification of FE-model for Gasket compression*, Report TFHF-5121, Lund University, Division of Solid Mechanics, Sweden 2006.
- [8] Gere J. and Goodno B., *Mechanics of Materials*, Seven edition, Cengage Learning 2009.
- [9] Austrell P.-E., *Modeling of Elasticity and Damping for Filled Elastomers*, Report TVSM-1009, Lund University, Division of Structural Mechanics, Sweden 1997.
- [10] *Columbia Encyclopedia sixth edition*, [www.infoplease.com/encyclopedia](http://www.infoplease.com/encyclopedia).
- [11] J.S. Dick, *How to Improve Rubber Compounds: 1500 Experimental Ideas for Problem Solving*, Hanser, Munich, 2004.
- [12] Håkansson P., Finite Element Modelling of a Rubber Block Exposed to Shock Loading, Report TFHF-5087, Lund University, Department of Mechanics and Materials, Sweden 2000.
- [13] Olsson A.K., Finite Element Procedures in Modelling the Dynamic Properties of Rubber, Report TVSM-1021, Lund University, Department of Construction Sciences, Sweden 2007.
- [14] Dolwichai P., Limtragool J., Inban S. and Piyasin S., *Hyperelastic Material Models for Finite Element Analysis with Commercial Rubber*, Technology and Innovation for Sustainable Development Conference (TISD2006), Faculty of engineering, Khon Kaen University, Thailand 2006
- [15] Wadham-Gagnon M., Hubert P., Semler Ch., Paidoussis M., Vézina M. and Lavoie D., *Hyperelastic Modeling of Rubber in Commercial Finite Element Software (ANSYS™)*, McGill University, Department of Mechanical engineering.
- [16] Renaud Ch. Cros J.-M., Feng Z.-Q. and Yang B., *The Yeoh Model Applied to the Modeling of Large Deformation*, *International Journal of Impact Engineering*, Elsevier, 2008.
- [17] Austrell P.-E., Stenbom B., Lindvall M. and Andersson L.-O., *Utveckling av Ändlägesdämpare för Bosch Rexroth Teknik AB*, Report TVSM-7140, Lund University, Department of Structural Mechanics, Sweden 2004.
- [18] *NHTSA people saving people*, [www.crashtest.com/explanations/nhtsa/usncap](http://www.crashtest.com/explanations/nhtsa/usncap).
- [19] *Tutorial on the Basics of Bolted Joints*, [www.boltscience.com](http://www.boltscience.com).

